

# Reusable Polyacrylonitrile-Sulfur Extractor of Heavy Metal Ions from Wastewater

Peng Li, Haibin Jiang, Ariel Barr, Zhichu Ren, Rui Gao, Hua Wang, Weiwei Fan, Meifang Zhu, Guiyin Xu,\* and Ju Li\*

Mercury, lead, and cadmium are among the most toxic and carcinogenic heavy metal ions (HMIs), posing serious threats to the sustainability of aquatic ecosystems and public health. There is an urgent need to remove these ions from water by a cheap but green process. Traditional methods have insufficient removal efficiency and reusability. Structurally robust, large surface-area adsorbents functionalized with high-selectivity affinity to HMIs are attractive filter materials. Here, an adsorbent prepared by vulcanization of polyacrylonitrile (PAN), a nitrogen-rich polymer, is reported, giving rise to PAN-S nanoparticles with cyclic  $\pi$ -conjugated backbone and electronic conductivity. PAN-S can be coated on ultra-robust melamine (ML) foam by simple dipping and drying. In agreement with hard/soft acid/base theory, N- and S-containing soft Lewis bases have strong binding to  $\text{Hg}^{2+}$ ,  $\text{Pb}^{2+}$ ,  $\text{Cu}^{2+}$ , and  $\text{Cd}^{2+}$ , with extraordinary capture efficiency and performance stability. Furthermore, the used filters, when collected and electrochemically biased in a recycling bath, can release the HMIs into the bath and electrodeposit on the counter-electrode as metallic  $\text{Hg}^0$ ,  $\text{Pb}^0$ ,  $\text{Cu}^0$ , and  $\text{Cd}^0$ , and the PAN-S@ML filter can then be reused at least 6 times as new. The electronically conductive PAN-S@ML filter can be fabricated cheaply and holds promise for scale-up applications.

## 1. Introduction

Heavy metal ions (HMIs) discharged from industrial processes (e.g., mining, steel, battery, electronic circuit board production, leather tanning, electroplating) and waste runoffs pose serious challenges for aquatic ecosystem sustainability and public health. Mercury, lead, and cadmium HMIs are extremely toxic, causing severe adverse effects on humans such as cancer, birth defects, mental retardation, kidney damage, as well as DNA damage from even trace level (ppb or ppt) HMIs exposure.<sup>[1–3]</sup> Industries face increasingly strict regulations for wastewater disposal to reduce the environmental impact of HMIs.<sup>[4]</sup> But HMIs still regularly exist in the natural environment and drinking water sources, especially in less-developed regions.<sup>[5,6]</sup> Several technologies have been pursued for the elimination of HMIs from polluted water, including chemical precipitation,<sup>[7,8]</sup> solvent extraction,<sup>[9,10]</sup> ion exchange,<sup>[11,12]</sup> and osmosis.<sup>[13]</sup> However, due to low removal efficiency, high treatment cost,

and the production of secondary pollutions, considerable work remains to be done. Especially when treating wastewater with relatively low HMI concentrations (US EPA limits are 0.002 mg (Hg)  $\text{L}^{-1}$ , 0.000 mg (Pb)  $\text{L}^{-1}$ , and 0.005 mg (Cd)  $\text{L}^{-1}$  for drinking water, or equivalently 2 ppb (Hg), 0 ppb (Pb), and 5 ppb (Cd)), the cost-efficacy envelope is often disappointing. Adsorption can have high uptake capacity, good selectivity, and fast kinetics, and thus provides a promising mechanism for HMIs decontamination.<sup>[14,15]</sup> Adsorbents that have been functionalized with matching metal-ion affinity groups and robust operation conditions (i.e., no stringent pH or post-processing requirements) are prerequisites.  $\text{Hg}^{2+}$ ,  $\text{Pb}^{2+}$ ,  $\text{Cu}^{2+}$ , and  $\text{Cd}^{2+}$  are Lewis soft acids, and possess stronger-binding compatibility with Lewis soft base groups, for example, RNC,  $\text{R}_2\text{S}$ , RSH, and  $\text{RS}^-$ , according to the hard/soft acid/base (HSAB) theory.<sup>[16]</sup> Based on this, nitrogen and sulfur-containing groups have been incorporated into organic/inorganic frameworks for  $\text{Hg}^{2+}$ ,  $\text{Pb}^{2+}$ ,  $\text{Cu}^{2+}$ , and  $\text{Cd}^{2+}$  metal ion removal.<sup>[17–23]</sup> The inorganic adsorbents, mainly amine-rich functionalized carbon material and metal sulfides, can be facilely synthesized and display high uptake capacity in the adsorption of these HMIs.<sup>[24–27]</sup> However, the deficiencies of low adsorption pH value, formation of  $\text{H}_2\text{S}$  gas, and the

P. Li

School of Environment Science and Spatial Informatics  
China University of Mining and Technology  
Xuzhou City, Jiangsu 221008, China


P. Li, H. Jiang, A. Barr, Z. Ren, R. Gao, H. Wang, W. Fan, G. Xu, J. Li  
Department of Nuclear Science and Engineering and Department of  
Materials Science and Engineering  
Massachusetts Institute of Technology  
Cambridge, MA 02139, USA  
E-mail: xuguiyin@mit.edu; liju@mit.edu

H. Jiang

SINOPEC Beijing Research Institute of Chemical Industry  
Beijing 100013, China

M. Zhu, G. Xu

State Key Laboratory for Modification of Chemical Fibers and Polymer  
Materials  
College of Materials Science and Engineering  
Donghua University  
Shanghai 201620, China

 The ORCID identification number(s) for the author(s) of this article can be found under <https://doi.org/10.1002/adfm.202105845>.

DOI: 10.1002/adfm.202105845

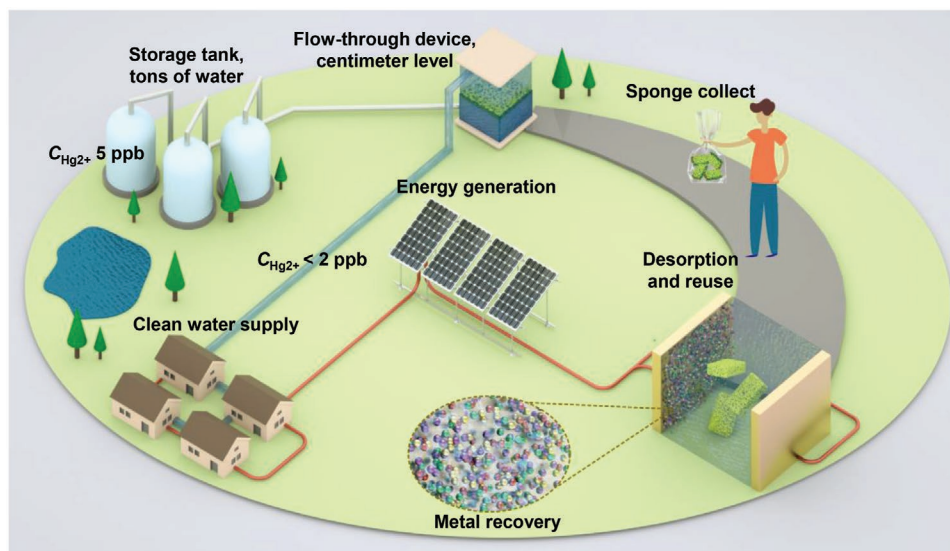


**Figure 1.** Schematic demonstrating of the HMIs polluted drinking water sources treatment and HMIs recovery with the proposed adsorption and electro-desorption method. First, tons of polluted water was drawn and stored as drinking water resource, a centimeter-level flow-through device packed with the fabricated PAN-S@ML sponge can in situ intercept the toxic HMIs quickly and efficiently, and the pass-through water with the HMIs concentration below 1.0 EPA can be supplied to the village. Then the PAN-S@ML sponge can be collected and regenerated with intermittent renewable energy, for example, solar photovoltaics. The PAN-S@ML sponge was desorbed with electro-desorption method along with the metal deposition in the cathode. The adsorbent can be reused, and the metal can be recovered simultaneously.

dissolution of active components restrict its widespread utilization. Among the organic adsorbents, thiol/thioether/pyridyl-based covalent/metal-organic frameworks show high uptake capacity for  $\text{Hg}^{2+}$ ,  $\text{Pb}^{2+}$ ,  $\text{Cu}^{2+}$ , and  $\text{Cd}^{2+}$  adsorption.<sup>[28–33]</sup> But due to high preparation cost, deterioration from corrosion, and inferior stability for reuse, thiol (-SH) containing COF or MOF are essentially unused in any practical wastewater treatment. Polymer-based adsorbents derived from in situ anchoring of exogenous Lewis basic sites show comparative ease in preparation and fine control of the adsorbent structure.<sup>[34–37]</sup> The reported *D*-limonene, canola oil, and dicyclopentadiene inverse vulcanized S-containing adsorbents have displayed easy preparation, large  $\text{Hg}^{2+}$  adsorption capacity, and tonne scale production.<sup>[38,39]</sup> However, it also shows poor desorption and recycling performance because of the strong affinity of the ionic bond formed between the HMIs and the Lewis base sites. Desorption is the reversal of adsorption, so strong adsorption is typically accompanied by insignificant desorption, necessitating a compromise between adsorption and desorption (if no voltage bias) for applications, and this lack of reusability increases the lifecycle cost of filtration. Unfortunately, relatively little attention has been dedicated to the desorption of HMIs, which leads to inferior reusability of the prepared adsorbents. Nanoscale adsorbent has been widely studied and pursued to obtain enlarged interfaces. The granulation or immobilization of the nanoparticle adsorbent will also be important for practical applications.

In this work, we report a highly porous, exceptionally stable, and easy-to-scale-up adsorbent grafted on industrially produced melamine (ML) foam, and a corresponding electro-desorption method for the elimination and recovery of multiple metal ions from wastewater. The ML foam consists of open-cell polymer fibers, and serves as a support for polyacrylonitrile-sulfur (PAN-S) nanoparticles that are the active component in water

filtration. The endogenous Lewis basic C–N, C=N, and exogenous C–S–S–C sites were generated through a simple thermal polymerization between polyacrylonitrile (PAN) and sulfur (S) powder. Interestingly, HMIs adsorption on PAN-S surface is selective, enabling the separation of  $\text{Hg}^{2+}$ ,  $\text{Pb}^{2+}$ ,  $\text{Cu}^{2+}$ , and  $\text{Cd}^{2+}$  from the other metal ions. More importantly, the polymeric PAN-S nanoparticle can be stably fastened onto the skeleton of ML sponge, which can withstand the filtration flow of HMI-containing water. After adsorption, the used sponges can be collected from various sites and moved to a central recycling bath, where the chemically adsorbed  $\text{Hg}^{2+}$ ,  $\text{Pb}^{2+}$ ,  $\text{Cu}^{2+}$ , and  $\text{Cd}^{2+}$  metals can be electrochemically desorbed, and reduced on the counter-electrode as metallic  $\text{Hg}^0$ ,  $\text{Pb}^0$ ,  $\text{Cu}^0$ , and  $\text{Cd}^0$  using electro-deposition, achieving the highest possible waste concentration. Both the adsorption and desorption processes are exceptionally robust, with almost no runoff or performance degradation over 6 adsorption-desorption cycles. This decentralized adsorption but centralized recycling and electrodeposition paradigm can greatly reduce the cost of drinking water detoxification (Figure 1).

## 2. Results and Discussion

### 2.1. Preparation of PAN-S Adsorbents and their Metal Ions Affinity

PAN-S nanoparticles were fabricated by a thermal polymerization method using nitrogen-rich polymer PAN as the matrix precursor and  $\text{S}_8$  powder as the S source (Figure S1a, Supporting Information). While pure PAN is an insulator, the sulfurized PAN gains cyclic conjugation as sulfur chains grafted onto the polymer, which makes PAN-S electronically conductive, a feature well exploited in lithium-sulfur batteries.<sup>[40,41]</sup>

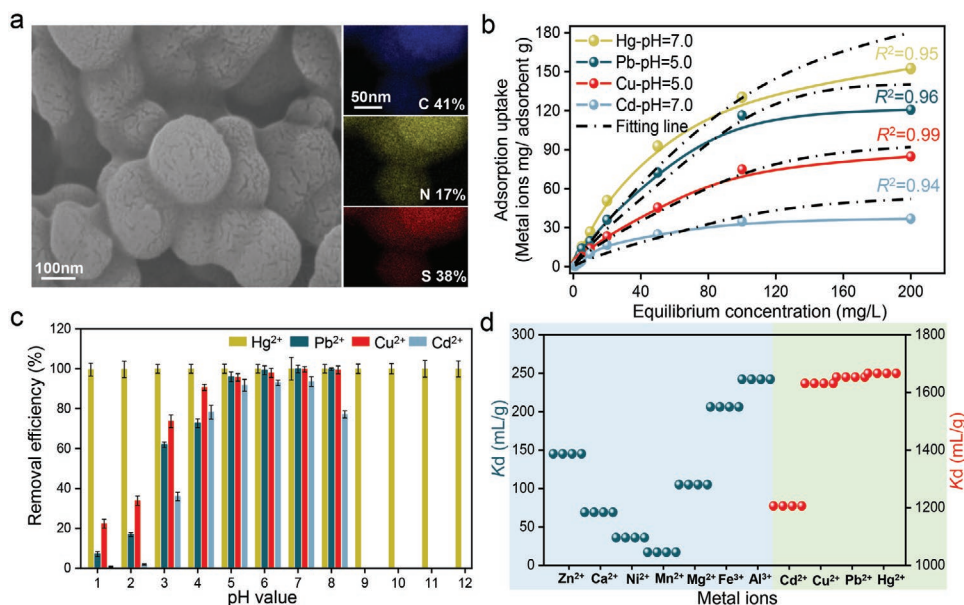


**Figure 2.** a) SEM and TEM-mapping images and the corresponding mass content of the prepared PAN-S nanoparticles, b) adsorption capacities for  $\text{Hg}^{2+}$ ,  $\text{Pb}^{2+}$ ,  $\text{Cu}^{2+}$ , and  $\text{Cd}^{2+}$ , c) adsorption performance at different solution pH, and d)  $K_d$  values for various metal ions. Experimental condition: (b) PAN-S dosage 30.0 mg, volume of wastewater 50 mL, adsorption duration 24 h, temperature 25 °C; (c) Metal ions initial concentration 2.0 mg L<sup>-1</sup>, PAN-S dosage 30.0 mg, volume of wastewater 50 mL, adsorption duration 2.0 h, temperature 25 °C; (d) Initial concentration 0.1 mg L<sup>-1</sup>, solution pH = 5.0, PAN-S dosage 30.0 mg, volume of wastewater 50 mL, adsorption duration 2.0 h, temperature 25 °C.

The micromorphology and particle size of the prepared PAN-S powder is shown in Figure 2a, and Figure S1b, Supporting Information, indicates connecting and binding between the nanoscale PAN-S particles of average size  $\approx 120$  nm. The relatively low polymerization temperature  $\approx 300$  °C permitted a reduced graphitization of the PAN substrate to prevent shrinkage and particle isolation.<sup>[40]</sup> The singly cross-linked PAN-S nanoparticles permit superior interface stability when used as an adsorbent in an aqueous solution.

The high-resolution transmission electron microscopy (HR-TEM) images in Figure S1c, Supporting Information, confirmed the agglomerated morphology and the nanoscale size of PAN-S particles. Poor crystallization of the PAN-S particles could be deduced from the irregular lattice diffraction. TEM-mapping images in Figure 2a revealed uniform distribution of N and S on the PAN-S nanoparticle surface, which provide an abundance of active sites (e. g. C–N, C=N, and C–S–S–C) for metal ion adsorption. The mass ratio of C, N, O, and S elements reflected from the mapping results was appropriately 41:17:4:38. The X-ray photoelectron spectroscopy (XPS) scanning spectra (Figure S2a, Supporting Information) of the PAN-S particle also showed that PAN-S mainly contains the elements C, N, O, and S, with a mass ratio of approximately 47:16:2:35, corroborating the TEM-mapping results. The XPS spectrum of high-resolution S scanning indicates confinement of S to C–S and S–S bonds (Figure S2b, Supporting Information). The binding energy peaks at 163.52 and 164.63 eV correspond to  $\text{S}2\text{p}_{3/2}$  and  $\text{S}2\text{p}_{1/2}$  orbitals in C–S bond, and the binding energy peaks at 161.68 and 162.79 eV signal the existence of  $\text{S}2\text{p}_{3/2}$  and  $\text{S}2\text{p}_{1/2}$  orbital in S–S bonds.<sup>[42,43]</sup> The C–S and S–S mass ratio calculated from the area in the high resolution S scanning spectra was 3.32:1. In the PAN-S structure, the C–S and S–S groups

tend to form a C–S–S–C covalent bond, which promotes S anchor stability.<sup>[44–46]</sup>

The high-resolution XPS scanning for N1s indicates that N exists in the form of C=N and C–N groups, as demonstrated by binding energy peaks at 399.96 and 398.18 eV, respectively (Figure S2c, Supporting Information).<sup>[47,48]</sup> The binding state of the N atom well matched its chemical configuration in the reported PAN-S molecule.<sup>[47]</sup> The Raman spectroscopy of the as-prepared PAN-S nanoparticles is shown in Figure S2d, Supporting Information. The strong characteristic peaks at 181 and 805 cm<sup>-1</sup> correspond to the C–S bond stretching, and the characteristic peaks at  $\approx 378$  cm<sup>-1</sup> are ascribed to in-plane bending of the C–S bond. The S–S bond can be identified by the peaks at 926 and 1157 cm<sup>-1</sup>, which are characteristic of the stretching of S–S bond containing rings, and the strong peaks at 1200 to 1600 cm<sup>-1</sup> are characteristic of carbon-like materials obtained by pyrolyzing a polymer. Owing to the relatively low synthesis temperature, characteristic peaks for elemental sulfur or poly(sulfur) can be found at 472 cm<sup>-1</sup>. The abundance of N and S bonds on the PAN-S nanoparticle surface provides an abundance of affinity sites for metal ions adsorption.<sup>[49–52]</sup>

The PAN-S nanoparticle displays outstanding affinity towards  $\text{Hg}^{2+}$ ,  $\text{Pb}^{2+}$ ,  $\text{Cu}^{2+}$ , and  $\text{Cd}^{2+}$  ions, with saturated adsorption capacity of 158.43, 120.68, 86.73, and 36.87 mg g<sup>-1</sup>, at solution pH of 7.0, 5.0, 5.0, and 7.0, respectively (Figure 2b). The uptake capacity of PAN-S was better than that of natural carbon, biomass, and synthetic clay adsorbents, though less than that of thiol (-SH) containing COF/MOF, and individual metal sulfide materials.<sup>[28,39,53,54]</sup> For example,  $\text{MoS}_2$  and ZnS nanoparticles have superior reported saturated adsorption capacities of 340 and 2000 mg g<sup>-1</sup>.<sup>[55,56]</sup> However, thiol (-SH) containing COF or MOF suffer from structural vulnerabilities,

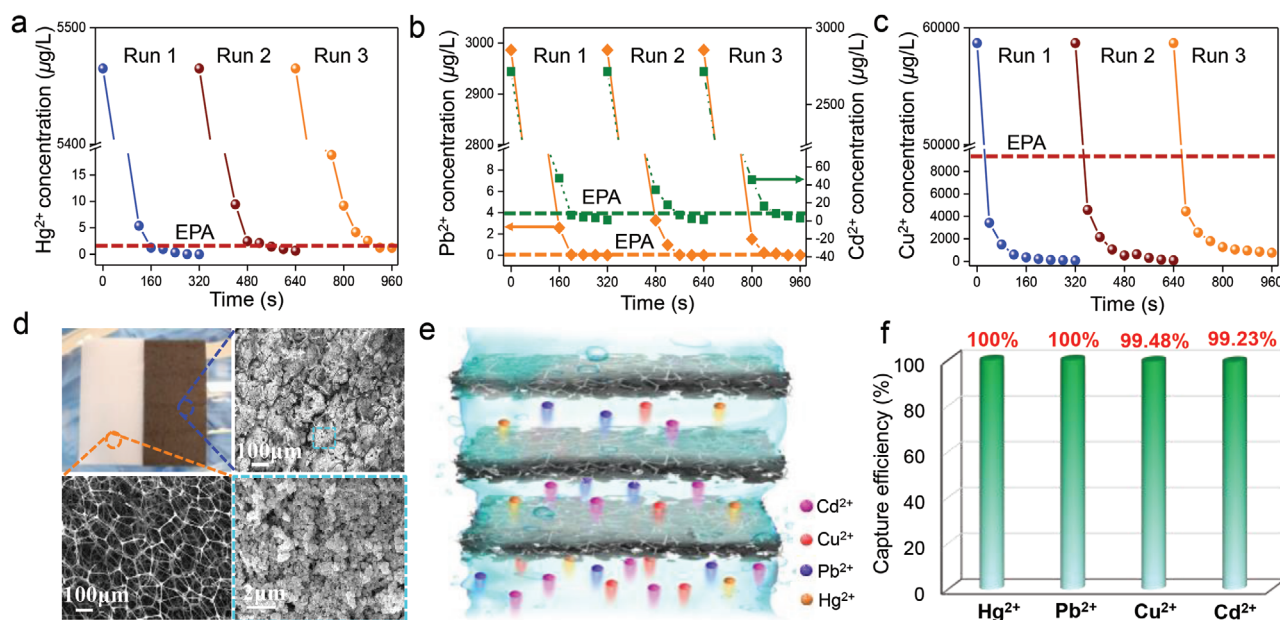


**Figure 3.** Concentration of a)  $\text{Hg}^{2+}$ , b)  $\text{Pb}^{2+}$  and  $\text{Cd}^{2+}$ , and c)  $\text{Cu}^{2+}$  during the flow-through adsorption, d) the digital photo and SEM images of pristine ML sponge and PAN-S@ML filter, e) the illustration for PAN-S@ML filter the flow-through adsorption method HMIs remove, and f)  $\text{Hg}^{2+}$ ,  $\text{Pb}^{2+}$ ,  $\text{Cu}^{2+}$ , and  $\text{Cd}^{2+}$  capture efficiency in the flow-through adsorption. Experimental condition:  $\text{Hg}^{2+}$ ,  $\text{Pb}^{2+}$ ,  $\text{Cu}^{2+}$ , and  $\text{Cd}^{2+}$  initial concentration  $\approx 5.0$ ,  $3.0$ ,  $60.0$ , and  $3.0 \text{ mg L}^{-1}$ , volume of the wastewater  $300 \text{ mL}$ , adsorption pH  $7.0$ ,  $5.0$ ,  $5.0$ , and  $7.0$ , repeated 3 times.

and have a narrow solution pH range for adsorption. In particular,  $\text{Hg}^{2+}$  is only adsorbed by the metal sulfide species under very acidic conditions ( $\text{pH} \approx 2.0\text{--}5.0$ ), and generates  $\text{H}_2\text{S}$  off-gas during the adsorption process. Continuous leaching of metal ions from the adsorbent will also occur, which results in inferior process stability. From this standpoint, PAN-S has superior performance owing to a wide range of pH operating conditions and excellent stability. The adsorption behavior of  $\text{Hg}^{2+}$ ,  $\text{Pb}^{2+}$ ,  $\text{Cu}^{2+}$ , and  $\text{Cd}^{2+}$  metal ions on PAN-S nanoparticle surface can be well-fitted with the Freundlich model, indicating a chemically dominant interaction.

The effect of solution pH on metal ion removal efficiency was comprehensively explored, and the results are shown in Figure 2c. The optimal solution pH for PAN-S metal ion uptake was appropriately 7.0, with uptake performance of  $\text{Pb}^{2+}$ ,  $\text{Cu}^{2+}$ , and  $\text{Cd}^{2+}$  dramatically increased in comparison with more acidic or alkaline conditions. The maximum removal efficiency for  $\text{Pb}^{2+}$ ,  $\text{Cu}^{2+}$ , and  $\text{Cd}^{2+}$  was 99.84%, 99.66%, and 93.55%, respectively. A high  $\text{Hg}^{2+}$  removal efficiency ( $>99.0\%$ ) was obtained in a broad solution pH range of 1.0 to 12.0, though the optimal adsorption still occurred at pH 7.0, where the removal efficiency reached 99.99%. This is ascribed to the saturate-coordinated N and S groups in PAN-S with an inferior affinity with  $\text{H}^+$ , thus the  $\text{S}\text{--}\text{Hg}^{2+}$  and  $\text{N}\text{--}\text{Hg}^{2+}$  ionic bond can break down the interaction between N, S, and  $\text{H}^+$ . Furthermore, for the reason of the relative weak affinity of N and S groups with  $\text{Pb}^{2+}$ ,  $\text{Cu}^{2+}$ , and  $\text{Cd}^{2+}$  ions, the solution pH dependence adsorption trends become apparent. When the adsorption occurred in a mixture, the  $\text{Hg}^{2+}$ ,  $\text{Pb}^{2+}$ ,  $\text{Cu}^{2+}$ , and  $\text{Cd}^{2+}$  ions are preferentially adsorbed with  $K_d$  values 1666, 1653, 1631, and 1206, respectively. The  $K_d$  values of  $\text{Hg}^{2+}$ ,  $\text{Pb}^{2+}$ ,  $\text{Cu}^{2+}$ , and  $\text{Cd}^{2+}$  ions were much larger than those of  $\text{Zn}^{2+}$ ,  $\text{Ca}^{2+}$ ,  $\text{Ni}^{2+}$ ,  $\text{Mn}^{2+}$ ,  $\text{Mg}^{2+}$ ,  $\text{Fe}^{3+}$ , and  $\text{Al}^{3+}$  species (detailed  $K_d$  values are listed in Table S1, Supporting

Information), which indicates that PAN-S nanoparticles capture  $\text{Hg}^{2+}$ ,  $\text{Pb}^{2+}$ ,  $\text{Cu}^{2+}$ , and  $\text{Cd}^{2+}$  ions with high selectivity when treated with mixture wastewater (Figure 2d). The outstanding preferential affinity for  $\text{Hg}^{2+}$ ,  $\text{Pb}^{2+}$ ,  $\text{Cu}^{2+}$ , and  $\text{Cd}^{2+}$  ions can be ascribed to the N and S function groups on PAN-S surface which possess a stronger affinity for soft Lewis acid HMIs.<sup>[57,58]</sup>

## 2.2. Preparation of PAN-S@ML Sponge Filter and their Metal Ions Affinity

As structural support for the water filter, we use the open porous ML foam (“Magic Eraser”). A very facile dipping and drying process into PAN-S ink can accomplish the synthesis of the PAN-S@ML sponge (Figure S3, Supporting Information). Due to the recyclability of N-methyl-pyrrolidinone (NMP) solvent, the process is cost-saving and sustainable. After the coating of PAN-S (with dilute polyvinylidene fluoride (PVDF) binder), the color of the white ML sponge changes to black. This indicates excellent coverage of PAN-S on the ML skeleton (formaldehyde-ML-sodium bisulfite copolymer) and electronic percolation. Interestingly, the PAN-S@ML filter (Figure 3d) inherits the porosity and skeletal structure of the parent ML sponge. The SEM images indicate that PAN-S nanoparticles are anchored onto the ML sponge skeleton structure while retaining rich pores structures at the same time. These pores structures provide abundant channels for wastewater flow-through in the sponge filter. It can be seen that the surface of the PAN-S@ML filter is covered with uniform nanoscale PAN-S particles. This unique structure promises good metal ion adsorption kinetics on the PAN-S@ML filter (Figure 3e). The nitrogen adsorption-desorption isotherms and the pore size distribution of different sponge materials are displayed in Figure S4, Supporting Information. The BET

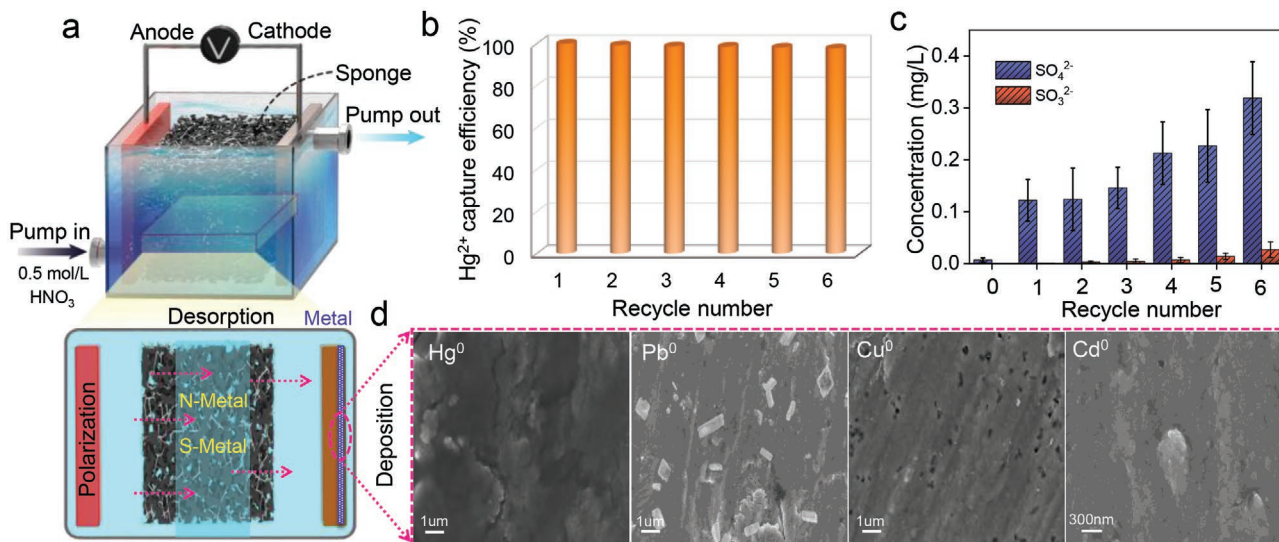


**Figure 4.** a) Detailed illustration of electrocatalytic desorption, b) Hg<sup>2+</sup> capture efficiency for the 6 cycles, c) the SO<sub>3</sub><sup>2-</sup> and SO<sub>4</sub><sup>2-</sup> concentration in the electrolyte, and d) Ti cathode surface after electro-desorption. Experimental condition: Hg<sup>2+</sup>, Pb<sup>2+</sup>, Cu<sup>2+</sup>, and Cd<sup>2+</sup> initial concentration ≈ 5.0, 3.0, 60.0, and 3.0 mg L<sup>-1</sup>, volume of the wastewater 300 mL, adsorption pH 7.0, 5.0, 5.0, and 7.0, repeated 3 times. Adsorption-desorption cycle 6 times.

surface area for the original sponge (Figure S4a, Supporting Information), PAN-S@ML filter, and PAN-S@ML filter after Hg<sup>2+</sup> adsorption was 9.87, 9.64, and 7.98 m<sup>2</sup> g<sup>-1</sup>, respectively. This indicates that the BET surface area has not increased after PAN-S attachment. The pore size distribution shown in Figure S4b, Supporting Information, indicates a decreased mesoporous structure after PAN-S attachment and metal ions adsorption. From the above, it can be deduced that a percolating PAN-S nanoparticles covered surface was formed. The adsorption on the PAN-S@ML filter surface can be ascribed to the porous framework structure and exposed PAN-S nanoparticles.

A self-made adsorption device with PAN-S@ML filter as packing material was constructed, and a metal-ion containing simulated wastewater batch treatment was conducted to evaluate the practicality of the proposed adsorption scheme, with results shown in Figure 3. As shown in Figure 3f, when high concentration Hg<sup>2+</sup>, Pb<sup>2+</sup>, Cu<sup>2+</sup>, and Cd<sup>2+</sup> metal-ion containing wastewater was treated in the first cycle, the capture efficiency was as high as 100.0%, 100.0%, 99.48%, and 99.23%, respectively. For the subsequent 3 repetitions, high concentration Hg<sup>2+</sup>, Pb<sup>2+</sup>, Cu<sup>2+</sup>, and Cd<sup>2+</sup> metal ions containing wastewater can still be purified to meet the EPA limit for drinking water within a very short 320 s duration (Figure 3a–c). The PAN-S nanoparticles provide an abundance of affinity sites for metal ion adsorption, which guarantees excellent HMI removal performance. Because a considerable percentage of the adsorbed metal ions are located on the surface of PAN-S@ML sponge, this platform provides a facile mechanism for the recycling of metal ions. The mass ratio of Cu on the PAN-S@ML filter surface reached 30.5% after 3 adsorption cycles (Figure S5, Supporting Information). As shown in Figure S6, Supporting Information, the mass ratio of Hg, Pb, and Cd on PAN-S@ML sponge surface after 3 adsorption repetitions was 26.2%, 34.3%, and 3.6%, respectively. The accumulated metal ions on the PAN-S@ML filter surface have significant potential for separation and reuse.

### 2.3. Zero-Valent Metal Recycling

An electrochemical method was explored for the desorption of Hg<sup>2+</sup>, Pb<sup>2+</sup>, Cu<sup>2+</sup>, and Cd<sup>2+</sup> metal ions from the PAN-S@ML filter surface. A detailed illustration of the electrochemical desorption is presented in Figure 4a. When a cell voltage (constant voltage 5.0 V) is applied, the N-metal and S-metal bonds formed between the PAN-S and HMIs will be broken due to electrolytic polarization. The desorbed Hg<sup>2+</sup>, Pb<sup>2+</sup>, Cu<sup>2+</sup>, and Cd<sup>2+</sup> metal ions will then be transmitted to the cathode and deposited as their corresponding zero-valent metallic form. A dilute 0.5 mol L<sup>-1</sup> HNO<sub>3</sub> was used as an electrolyte for the dissolution of Hg<sup>2+</sup>, Pb<sup>2+</sup>, Cu<sup>2+</sup>, and Cd<sup>2+</sup> metal ions. The current used during the electrochemical desorption was quite small (0.08 A), and therefore, only a small amount of electric power is required during the desorption. The adsorption-desorption treatment was continuously performed for 6 cycles, with amazing performance stability. An average capture efficiency for Hg<sup>2+</sup> was maintained at 97.72%, suffering only 2.28% attenuation in comparison with the first recycle at 100.0% (Figure 4b).

The concentration of SO<sub>3</sub><sup>2-</sup> and SO<sub>4</sub><sup>2-</sup> in the electrolyte was monitored to understand the S runoff behavior during PAN-S@ML filter desorption, with results shown in Figure 4c. The concentration of SO<sub>3</sub><sup>2-</sup> and SO<sub>4</sub><sup>2-</sup> in the electrolyte was low, even following 6 adsorption-desorption cycles, the outlets SO<sub>3</sub><sup>2-</sup> and SO<sub>4</sub><sup>2-</sup> were still only 0.319 and 0.027 mg L<sup>-1</sup>. This is significantly below the 250 mg L<sup>-1</sup> sulfate limit for public water systems. This result indicates that the S species in the PAN-S framework was stably anchored with almost no losses occurring during the electrocatalytic oxidation. Hence, a stable adsorption-desorption process for Hg<sup>2+</sup>, Pb<sup>2+</sup>, Cu<sup>2+</sup>, and Cd<sup>2+</sup> metal ions on the PAN-S@ML sponge can be realized. The mass content of Hg<sup>2+</sup>, Pb<sup>2+</sup>, Cu<sup>2+</sup>, and Cd<sup>2+</sup> metal ions on PAN-S@ML sponge decreases dramatically to a very low level of 3.9%, 1.6%, 2.3%, and 0.3% after the electrochemical recycling treatment (Figures S6 and S7, Supporting Information), indicating high

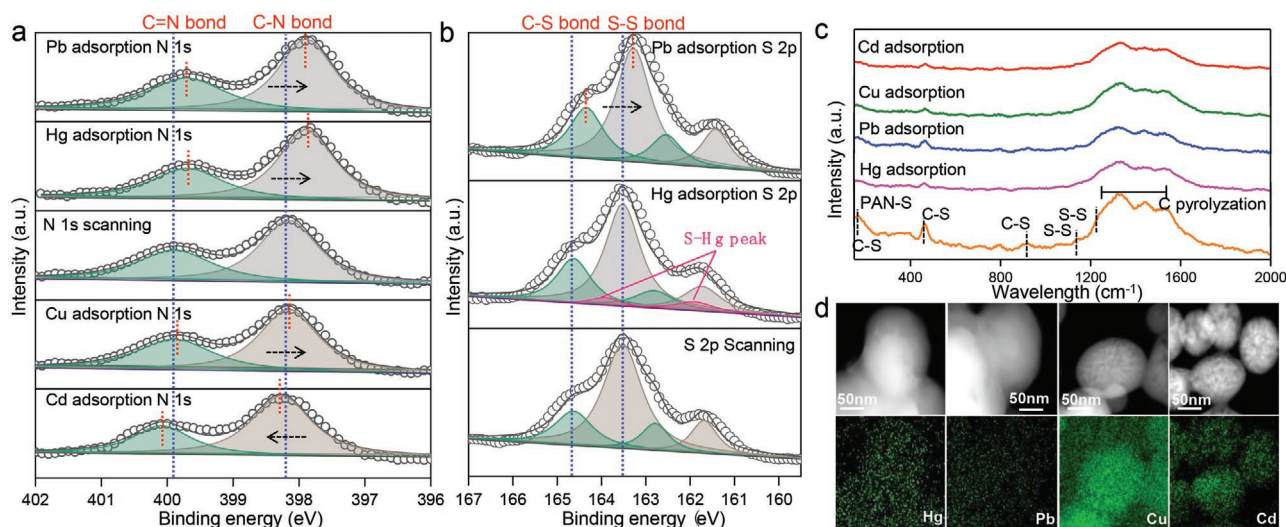


**Figure 5.** High-resolution XPS spectra of a) N 1s and b) S 2p before and after metal ions adsorption, c) Raman spectroscopy of original PAN-S nanoparticles and after  $\text{Hg}^{2+}$ ,  $\text{Pb}^{2+}$ ,  $\text{Cu}^{2+}$ , and  $\text{Cd}^{2+}$  adsorption, and d) TEM-mapping images of PAN-S nanoparticles after  $\text{Hg}^{2+}$ ,  $\text{Pb}^{2+}$ ,  $\text{Cu}^{2+}$ , and  $\text{Cd}^{2+}$  metal ion adsorption. Experimental condition: metal ions concentration  $10.0 \text{ mg L}^{-1}$ ,  $\text{pH} = 5.0$ , PAN-S dosage  $30.0 \text{ mg}$ , volume of wastewater  $50 \text{ mL}$ , adsorption duration  $24.0 \text{ h}$ , and temperature  $25 \text{ }^\circ\text{C}$ .

desorption efficiency. Compared to the insignificant desorption performance obtained with direct  $0.5 \text{ mol L}^{-1} \text{ HNO}_3$  elution for PAN-S@ML sponge  $\text{Cu}^{2+}$  desorption, electro-desorption is an effective method to separate HMIs from PAN-S@ML sponge surface (Figure S8, Supporting Information). The SEM images of the Ti cathode following the electrocatalytic desorption (Figure 4d and Figure S9, Supporting Information) show that elemental  $\text{Hg}^0$ ,  $\text{Pb}^0$ ,  $\text{Cu}^0$ , and  $\text{Cd}^0$  were obtained, which is the most compact and least hazardous waste form possible. Despite this success, purifying catchment or tailings dam wastewater containing significant amounts of organic matter (such as humic matter) should be further explored.<sup>[59]</sup>

## 2.4. HMIs Extraction Mechanism

The extraction mechanism for  $\text{Hg}^{2+}$ ,  $\text{Pb}^{2+}$ ,  $\text{Cu}^{2+}$ , and  $\text{Cd}^{2+}$  metal ions from water solution with PAN-S adsorbents was explored with XPS analysis, Raman spectroscopy, and TEM mapping. From the XPS spectra after the  $\text{Hg}^{2+}$ ,  $\text{Pb}^{2+}$ ,  $\text{Cu}^{2+}$ , and  $\text{Cd}^{2+}$  adsorption, characteristic spectra for the metal species were observed (Figure S10, Supporting Information). Specifically, the Hg 4f at  $100.81 \text{ eV}$ , the Pb 4f at  $138.19 \text{ eV}$ , the Cu 2p at  $932.02 \text{ eV}$ , and the Cd 3d at  $418.30 \text{ eV}$ . And the surface accumulation of  $\text{Hg}^{2+}$ ,  $\text{Pb}^{2+}$ ,  $\text{Cu}^{2+}$ , and  $\text{Cd}^{2+}$  metal ions can be seen from the TEM mapping (Figure 5d), which illustrates that metal ions were adsorbed and accumulated on the surface of the PAN-S nanoparticles. There are dramatic changes between the C–N, C=N, and –C–S–S–C– bonds before and after metal ion adsorption as described in XPS spectra, the details of which are shown in Figure 5 and Figure S11, Supporting Information.

After  $\text{Hg}^{2+}$  adsorption, the binding energy peaks for C=N and C–N decreased from  $399.96$  and  $398.18 \text{ eV}$  to  $399.69$  and  $397.84 \text{ eV}$ , respectively, indicating the affinity between C=N, C–N, and  $\text{Hg}^{2+}$ .<sup>[31,60–62]</sup> Compared with the C=N binding energy change ( $-0.27 \text{ eV}$ ), the C–N bond energy change

( $-0.34 \text{ eV}$ ) was more significant, indicating that  $\text{Hg}^{2+}$  has a greater affinity for C–N bonds than C=N (Figure 5a). The C–S–S–C group also experienced significant changes after  $\text{Hg}^{2+}$  accumulation, as shown in Figure 5b. The binding energy peak of S  $2p_{3/2}$  from the C–S bond and the binding peak of S  $2p_{3/2}$  from the S–S bond (originally at  $163.52$  and  $161.68 \text{ eV}$ ) greatly decreased, especially the peak of the S–S bond. The area of the binding energy peak shrank dramatically to around half that of pristine PAN-S, which can be ascribed to the breaking of S–S bonds during  $\text{Hg}^{2+}$  adsorption. The formation of S–Hg bonds can be identified from the S  $2p_{3/2}$  and S  $2p_{1/2}$  binding energy peaks at  $161.90$  and  $163.91 \text{ eV}$ .<sup>[63]</sup> The affinity mechanism between PAN-S and  $\text{Hg}^{2+}$  can be described as occurring due to entrapment of  $\text{Hg}^{2+}$  by C=N, C–N, C–S, and S–S via electrostatic affinity, with S–S bond breakage resulting from stronger interaction between S and  $\text{Hg}^{2+}$  during adsorption.

The  $\text{Hg}^{2+}$ ,  $\text{Pb}^{2+}$ ,  $\text{Cu}^{2+}$ , and  $\text{Cd}^{2+}$  metal ions displayed different adsorption properties based on their interaction performance with PAN-S nanoparticles. For  $\text{Pb}^{2+}$  adsorption, the binding energy peaks for C=N and C–N at  $399.96$  and  $398.18 \text{ eV}$  decreased to  $399.70$  and  $397.89 \text{ eV}$ .<sup>[64,65]</sup> The binding energy peak of S  $2p_{3/2}$  belonging to C–S and S–S bonds decreased from  $163.52$  and  $161.68 \text{ eV}$  to  $163.28$  and  $161.42 \text{ eV}$ . An insignificant decrease in the binding energy peak for S–S bond was observed, which may indicate the affinity of S–Pb was not sufficient to break the S–S bond on PAN-S framework. For  $\text{Cu}^{2+}$  adsorption, change in the N 1s binding energy peak was also observed, decreasing from  $399.96$  and  $398.18 \text{ eV}$  to  $399.89$  and  $398.12 \text{ eV}$ .<sup>[66,67]</sup> Following  $\text{Cd}^{2+}$  adsorption, the binding energy peaks for C=N and C–N increased slightly to  $400.08$  and  $398.27 \text{ eV}$ , and the S–Cd bond can be found through S  $2p_{3/2}$  and S  $2p_{1/2}$  scanning at binding energy peaks of  $161.80$  and  $162.78 \text{ eV}$ .<sup>[68,69]</sup> This provides obvious evidence for  $\text{Cd}^{2+}$  adsorption by C=N, C–N, and C–S–S–C groups. Nevertheless, the C=N and C–N bond binding energy changes were much smaller than for  $\text{Hg}^{2+}$ ,  $\text{Pb}^{2+}$ , and  $\text{Cu}^{2+}$  adsorption. This

can be ascribed to the relatively weak affinity between PAN-S and  $\text{Cd}^{2+}$  as compared with  $\text{Hg}^{2+}$ ,  $\text{Pb}^{2+}$ , and  $\text{Cu}^{2+}$ .

The high-resolution XPS spectra for Hg 4f, Pb 4f, Cu 2p, and Cd 3d on the PAN-S surface are displayed in Figure S10a, Supporting Information. The Hg 4f binding energy yields two peaks from Hg 4f<sub>7/2</sub> and Hg 4f<sub>5/2</sub> at 100.81 and 104.86 eV, as expected from the initial Hg +2 state. The Hg 4f<sub>7/2</sub> spectrum is a composite of two peaks with binding energy of 100.38 and 100.98 eV, while the Hg 4f<sub>5/2</sub> spectrum can be divided into two distinct peaks 104.46 and 105.05 eV, which indicate the existence of N–Hg and S–Hg bonds, respectively.<sup>[31]</sup> The observed Hg atom binding energy states correspond to N and S bonded Hg, demonstrating that the C=N, C–N, and C–S–S–C functional groups have a strong affinity for  $\text{Hg}^{2+}$ . The Raman spectroscopy of the original PAN-S nanoparticle and after  $\text{Hg}^{2+}$ ,  $\text{Pb}^{2+}$ ,  $\text{Cu}^{2+}$ , and  $\text{Cd}^{2+}$  adsorption (Figure 5c) showed that the C–S and S–S peak on PAN-S surface decrease obviously, which provides evidence of  $\text{Hg}^{2+}$ ,  $\text{Pb}^{2+}$ ,  $\text{Cu}^{2+}$ , and  $\text{Cd}^{2+}$  adsorption on PAN-S surface.

Based on the analysis above, the mechanism for  $\text{Hg}^{2+}$ ,  $\text{Pb}^{2+}$ ,  $\text{Cu}^{2+}$ , and  $\text{Cd}^{2+}$  metal ions adsorption with PAN-S nanoparticles can be deduced: the soft base groups of C–N, C=N, and C–S–S–C have a strong affinity with soft acid  $\text{Hg}^{2+}$ ,  $\text{Pb}^{2+}$ ,  $\text{Cu}^{2+}$ , and  $\text{Cd}^{2+}$  species. The proposed mechanism is illustrated in Figure S10c, Supporting Information. The more the soft acid character, the stronger the adsorption behavior;  $\text{Hg}^{2+}$  adsorption can also lead to the breakdown of S–S bonds in the C–S–S–C group.

## 2.5. Techno-Economics and Environmental Sustainability

The components for PAN-S@ML sponge filter production are green and cost-efficient. Cumulative economic demand and environmental sustainability were analyzed to evaluate the potential scalability of the proposed adsorption and electro-desorption method. The amount of PAN-S nanoparticle for one batch for treating of 5.4 L  $\text{Hg}^{2+}$  containing water (concentration 5,000 ppb) was 8.0 g. The corresponding cost for PAN-S and PAN-S@ML preparation and the cost for the electrodes and electricity were all calculated and the total was 30.37 US \$. The detailed cost is listed in Table S2, Supporting Information. Besides, in consideration of the recycling possibility of NMP, the cost will be reduced in practical production. The initial  $\text{Hg}^{2+}$ ,  $\text{Pb}^{2+}$ ,  $\text{Cu}^{2+}$ , and  $\text{Cd}^{2+}$  concentration of the scattered drinking water intake point for the rural villages was assumed to be 5, 5, 10, and 1500 ppb, and the discharge standard was 2, 0, 5, and 1300 ppb, respectively. The treatment cost of the  $\text{Hg}^{2+}$ ,  $\text{Pb}^{2+}$ ,  $\text{Cu}^{2+}$ , and  $\text{Cd}^{2+}$  contaminated surface/groundwater was 0.17, 0.47, 0.94, and 0.94 US \$/ton, which was low and competitive with the currently applied techniques (displayed in Figure S12, Supporting Information). These calculations prove the economic and environmental feasibility of the proposed adsorption and electro-desorption method for HMIs elimination and recovery.

## 3. Conclusion

In this work, we have demonstrated a sustainable, affordable, and easily implemented adsorbent preparation, as well as an

ultra-robust and stable electrochemical recycling strategy for the highly efficient removal and recovery of  $\text{Hg}^{2+}$ ,  $\text{Pb}^{2+}$ ,  $\text{Cu}^{2+}$ , and  $\text{Cd}^{2+}$  from wastewater. Our approach involves the in situ generation of endogenous Lewis basic C–N, C=N, and C–S–S–C affinity sites on PAN-S nanoparticles and the immobilization of the prepared nanoparticle adsorbent on a mechanically robust ML foam. A simple thermal polymerization between PAN and sulfur powder was introduced for the preparation of PAN-S, which displayed extensive pH ( $\approx 1.0$ – $12.0$ ) competence for  $\text{Hg}^{2+}$  adsorption and selective adsorption for  $\text{Hg}^{2+}$ ,  $\text{Pb}^{2+}$ ,  $\text{Cu}^{2+}$ , and  $\text{Cd}^{2+}$  HMIs. A facile dipping and drying process could accomplish the stably fasten PAN-S onto the skeletal surface of ML sponge, the fabricated PAN-S@ML filter then inherited the porosity of ML sponge permitting the flow-through of wastewater and interception of the HMIs with the exposed affinity sites. The capture efficiency for  $\text{Hg}^{2+}$ ,  $\text{Pb}^{2+}$ ,  $\text{Cu}^{2+}$ , and  $\text{Cd}^{2+}$  containing wastewater with an initial concentration of 5.0, 3.0, 60.0, and 3.0 mg L<sup>-1</sup> was measured to be 100.0%, 100.0%, 99.48%, and 99.23%, and the outlet all met the US EPA requirement for drinking, with very low sulfur runoff. And the mass ratio of the accumulated  $\text{Hg}^{2+}$ ,  $\text{Pb}^{2+}$ ,  $\text{Cu}^{2+}$ , and  $\text{Cd}^{2+}$  on the PAN-S@ML filter was as high as 26.2%, 34.3%, 3.6%, and 30.5%, respectively, indicating excellent usage of affinity sites. The HMIs can be collected from the wastewater and accumulated for significant recovery. Importantly, the PAN-S@ML filter could be regenerated with an electrocatalytic desorption method, and metallic states of  $\text{Hg}^0$ ,  $\text{Pb}^0$ ,  $\text{Cu}^0$ , and  $\text{Cd}^0$  covered the surface of the counter electrode. Both the adsorption and desorption were exceptionally stable with nearly no attenuation after 6 cycles. The components for PAN-S@ML sponge production are green and cost-effective, which offer a sustainable and affordable approach to the recovery of HMIs from wastewater and opens a promising avenue towards drinking water treatment.

## 4. Experimental Section

**PAN-S Nanoparticle Preparation:** In a typical synthesis of the PAN-S nanoparticles, 6.0 g PAN (Sigma-Aldrich, USA) and 24.0 g sulfur powder (Sigma-Aldrich, USA) were mixed and ground together. The powder was then sintered under argon atmosphere following a three-step thermal treatment procedure of: 1) heating from 20 to 300 °C at a constant heating rate of 3.0 °C min<sup>-1</sup>, 2) maintain the temperature at 300 °C for 10 h, and 3) cooled from 300 °C to room temperature at a constant cooling rate of 3.0 °C min<sup>-1</sup>. The as-prepared carbon polymer was then fully ground to obtain decentralized nanoparticles. The yield of PAN-S nanoparticles was 28.3%.

**PAN-S@ML Sponge Filter Fabrication:** For the fabrication of the PAN-S@ML sponge filter, 0.8 g PVDF (Sigma-Aldrich, USA) was dissolved in 80 g NMP (Sigma-Aldrich, USA) with vigorous stirring for 4.0 h at a constant temperature of 80 °C. After cooling to room temperature, PAN-S nanoparticles (8.0 g) were added to the NMP solution and dispersed as a black-crosslinking slurry. Then the commercial ML foam (with exterior size of 60.0×20.0×2.0 mm) was dipped into the slurry for 2.0 min, and air-dried to constant weight at 60 °C in oven.

**Bulk Metallic Wastewater Adsorption:** The  $\text{Hg}^{2+}$ ,  $\text{Pb}^{2+}$ ,  $\text{Cu}^{2+}$ , and  $\text{Cd}^{2+}$  adsorption capacity of the as-prepared PAN-S nanoparticles and PAN-S@ML sponge was comprehensively investigated. The optimum solution pH, selective affinities for  $\text{Hg}^{2+}$ ,  $\text{Pb}^{2+}$ ,  $\text{Cu}^{2+}$ , and  $\text{Cd}^{2+}$  ions, and corresponding saturated adsorption capacities (*q*) were obtained for PAN-S nanoparticles. Systematic flow-through experiments were conducted using a self-designed device (Figure S13a, Supporting

Information) packed with PAN-S@ML sponge, and high metal ion concentration (5.0 mg L<sup>-1</sup> of Hg<sup>2+</sup>, 3.0 mg L<sup>-1</sup> of each Pb<sup>2+</sup> and Cd<sup>2+</sup>, and 60.0 mg L<sup>-1</sup> of Cu<sup>2+</sup>).

Feasibility of metal ion recovery from the PAN-S@ML sponge was explored using an electrolytic-desorption process with 150 mL 0.5 mol L<sup>-1</sup> HNO<sub>3</sub> as electrolyte (Figure S13b, Supporting Information). Operational details of the experimental wastewater treatment and ion recovery method are shown in Figure S1, Supporting Information. The optimum solution pH for Hg<sup>2+</sup>, Pb<sup>2+</sup>, Cu<sup>2+</sup>, and Cd<sup>2+</sup> ion adsorption was investigated using 2.0 mg L<sup>-1</sup> initial ion concentration, a 30 mg PAN-S nanoparticle dosage added to 50 mL simulated wastewater, and 2.0 h adsorption duration at 25 °C in a water bath shaker. For Hg<sup>2+</sup>, controlled investigation of pH-dependent adsorption was conducted for the pH range 1.0 to 12.0 in increments of 1.0. Similarly, for Pb<sup>2+</sup>, Cu<sup>2+</sup>, and Cd<sup>2+</sup>, the pH range 1.0 to 8.0 was investigated in increments of 1.0.

Wastewater containing various metal ions, including Hg<sup>2+</sup>, Pb<sup>2+</sup>, Cu<sup>2+</sup>, Cd<sup>2+</sup>, Zn<sup>2+</sup>, Ca<sup>2+</sup>, Ni<sup>2+</sup>, Mn<sup>2+</sup>, Mg<sup>2+</sup>, Fe<sup>3+</sup>, and Al<sup>3+</sup>, was used to evaluate selective affinity for Hg<sup>2+</sup>, Pb<sup>2+</sup>, Cu<sup>2+</sup>, and Cd<sup>2+</sup> ions. The solution pH was controlled to be 5.0, and the initial concentration of each ionic species was maintained at 100.0 µg L<sup>-1</sup>. The mixture was set aside for 24 h, then passed through a 0.22 µm filter membrane. The result of this process was then treated as the initial solution in the adsorption experiments. For the adsorption experiments, a 30 mg dosage of PAN-S nanoparticles was added to 50 mL of simulated wastewater for a duration of 2.0 h at 25 °C in a water bath shaker. The affinity of PAN-S particles towards HMIs can be expressed in terms of the distribution coefficient ( $K_d$ , mL g<sup>-1</sup>) as given by the following equation:

$$K_d = \frac{c_0 - c_e}{c_e} \left( \frac{V}{M} \right) \quad (1)$$

where  $c_0$  and  $c_e$  are the initial and terminal metal ions concentrations, mg L<sup>-1</sup>;  $V$  the total volume of the solution, mL; and  $M$  the mass of the added PAN-S nanoparticles, g.

The saturated adsorption capacity ( $q$ ) of PAN-S nanoparticles for Hg<sup>2+</sup>, Pb<sup>2+</sup>, Cu<sup>2+</sup>, and Cd<sup>2+</sup> ions were investigated using initial metal ion concentration wastewater prepared as 1.0, 2.0, 3.0, 4.0, 5.0, 10.0, 20.0, 50.0, 100.0, and 500.0 mg L<sup>-1</sup>. It was worth noting that the solution pH was controlled at different values for Hg<sup>2+</sup>, Pb<sup>2+</sup>, Cu<sup>2+</sup>, and Cd<sup>2+</sup> adsorption because the ions have different pH-dependent dissociation properties. The solution pH used for Hg<sup>2+</sup>, Pb<sup>2+</sup>, Cu<sup>2+</sup>, and Cd<sup>2+</sup>  $q$  measurements was 7.0, 5.0, 5.0, and 7.0, respectively, where the  $q$  value has been calculated using the following equation:

$$q = \frac{(c_0 - c_e) \times V}{M} \quad (2)$$

Systematic flow-through treatment with metal ion recovery experiments was conducted to evaluate the applicability of the proposed scheme. The self-designed flow-through adsorption and electrolytic-desorption devices were prepared with 3D-printed parts using polylactic acid plastics (PLA). The as-prepared PAN-S@ML sponge was employed as filling material to fabricate a flow-through adsorption device for the efficient treatment of high metal ion concentration wastewater with initial Hg<sup>2+</sup> concentration 5.0 mg L<sup>-1</sup>, Pb<sup>2+</sup> and Cd<sup>2+</sup> 3.0 mg L<sup>-1</sup>, and Cu<sup>2+</sup> 60.0 mg L<sup>-1</sup> using 300.0 mL solution volume. Flow-through treatment was conducted 3 times under the same experimental conditions. The concentration of different metal ions was determined with inductively coupled plasma mass spectrometry (ICP-MS, Agilent 7900, USA). And the highest standard solution for Hg<sup>2+</sup> detection was 200 ppb. It was worth noting that on account of the precipitation phenomenon that occurs in high metal ion concentration solutions, control of pH in the flow-through device was vital. To that end, the species distribution of Hg<sup>2+</sup>, Pb<sup>2+</sup>, Cu<sup>2+</sup>, and Cd<sup>2+</sup> as a function of pH was calculated using the software Visual MINTEQ ver 3.1, assuming an ionic strength of 0.2 mol L<sup>-1</sup>, and NO<sub>3</sub><sup>-</sup> concentration of 0.05 mol L<sup>-1</sup>, with results shown in Figure S14, Supporting Information. Based on the results from the species distribution simulation, the controlled pH values for Hg<sup>2+</sup>, Pb<sup>2+</sup>, Cu<sup>2+</sup>, and Cd<sup>2+</sup> flow-through adsorption were 7.0, 5.0, 5.0, and 7.0, respectively.

**Metal Ion Recovery:** Regeneration of the PAN-S@ML sponge filter was conducted using an electrochemical process in a self-designed PLA reactor. In this process, the used PAN-S@ML sponge was packed in-between the electrodes, where graphite and titanium plate served as anode and cathode, respectively. The size of the electrode was 60.0 mm × 60.0 mm × 2.0 mm, and the distance between anode and cathode was 25.0 mm. The desorption treatment employed 150 mL of 0.5 mol L<sup>-1</sup> concentration nitric acid as the electrolyte, with a voltage of 5.0 V, for a duration of 0.5 h. After treatment, 0.15 mL of formaldehyde and 2.0 mL of 0.1 mol L<sup>-1</sup> ethylenediaminetetraacetic acid was added to the electrolyte solution, and ion chromatography (IC, Thermo ICS-2100, UAS, with AS11-HC anion column) was employed to measure concentrations of SO<sub>3</sub><sup>2-</sup> and SO<sub>4</sub><sup>2-</sup>.

**Material Characterization:** The morphology and the element distribution of the PAN-S nanoparticle and PAN-S@ML filter before and after ion adsorption was observed by field emission scanning electron microscopy (FE-SEM, ZEISS SUPRA 40, Germany), HR-TEM (Tecnai G2 F20, FEI, USA), and X-Ray energy dispersive spectroscopy (EDS-Mapping, SuperX, FEI, USA). The specific surface area of the synthetic PAN-S@ML sponge was determined according to the Brunauer–Emmett–Teller (BET) model and the pore size distribution was calculated via the Barrett–Joyner–Halenda (BJH) method using a micromeritics TriStar II Plus surface area analyzer (Micro, ASAP 2020, USA). The lattice structure, phase composition, and surface groups were recorded using X-ray diffraction (XRD, Bruker D8, Germany), and Fourier transform infrared spectroscopy (FT-IR, Nicolet-460, USA), with changes in the chemical and electronic states of N, S, and metal atoms detected using XPS (K-Alpha, USA). The cathode (Ti plate) before and after the electrolytic-desorption process was comprehensively characterized using FE-SEM and EDS-Mapping methods.

## Supporting Information

Supporting Information is available from the Wiley Online Library or from the author.

## Acknowledgements

The authors would like to acknowledge the support of Yintai Investment Co., LLC. B.M.

## Conflict of Interest

The authors declare no conflict of interest.

## Data Availability Statement

Research data are not shared.

## Keywords

drinking water filters, electro-desorption, metal recovery, recycling, soft lewis acids

Received: June 17, 2021  
Revised: July 22, 2021  
Published online: August 27, 2021

[1] Y. Chen, M. J. Xu, J. Y. Wen, Y. Wan, Q. F. Zhao, X. Cao, Y. Ding, Z. L. Wang, H. X. Li, Z. F. Bian, *Nat. Sustain.* **2021**, *4*, 618.



- [2] B. Y. Li, Y. M. Zhang, D. X. Ma, Z. Shi, S. Q. Ma, *Nat. Commun.* **2014**, *5*, 5537.
- [3] A. Joy, A. Qureshi, *Environ. Sci. Technol.* **2020**, *54*, 14139.
- [4] World Health Organization. Drinking-Water Fact-Sheet, <https://www.epa.gov/ground-water-and-drinking-water/national-primary-drinking-water-regulations> (accessed: January 2021).
- [5] The hindu center of politics and public policy. Heavy metals contaminating India's rivers: Samples from 65% of testing sites unsafe: survey, <https://www.thehindu.com/news/national/heavy-metals-contaminating-indias-rivers/article30279681.ece> (accessed: December 2019).
- [6] UN environment programme. The Caribbean Environment Programme (CEP). Global versus Caribbean Studies on Mercury, Lead and Cadmium, <https://www.unep.org/cep/heavy-metals>.
- [7] X. Vecino, M. Reig, J. López, C. Valderrama, J. L. Cortina, *J. Environ. Manage.* **2021**, *283*, 112004.
- [8] H. Y. Wu, W. J. Wang, Y. F. Huang, G. H. Han, S. Z. Yang, S. P. Su, H. Sana, W. J. Peng, Y. J. Cao, J. T. Liu, *J. Hazard. Mater.* **2019**, *371*, 592.
- [9] J. M. Nan, D. M. Han, X. X. Zuo, *J. Power Sources* **2005**, *152*, 278.
- [10] M. C. Aragoni, M. Arac, A. Bencini, S. Biagini, A. J. Blake, C. Caltagirone, F. Demartin, F. G. De, F. A. Devillanova, A. Garau, *Inorg. Chem.* **2008**, *47*, 8391.
- [11] P. Goyal, C. S. Tiwary, S. K. Misra, *J. Environ. Manage.* **2021**, *277*, 111469.
- [12] Y. Ibrahim, V. Naddeo, F. Banat, S. W. Hasan, *Sep. Purif. Technol.* **2020**, *250*, 117250.
- [13] M. L. He, L. Wang, Y. T. Lv, X. D. Wang, J. N. Zhu, Y. Zhang, T. T. Liu, *Chem. Eng. J.* **2020**, *389*, 124452.
- [14] K. Gai, A. Avellan, T. P. Hoelen, F. L. Linares, E. S. Hatakeyama, G. V. Lowry, *Water Res.* **2019**, *157*, 600.
- [15] C. C. Long, X. Li, Z. X. Jiang, P. Zhang, Z. H. Qing, T. P. Qing, B. Feng, *J. Hazard. Mater.* **2021**, *413*, 125470.
- [16] R. G. Pearson, *Chemical hardness*, Wiley-Vch, Verlag GmbH, Weinheim **1997**.
- [17] D. T. Sun, L. Peng, W. S. Reeder, S. M. Moosavi, D. Tiana, D. K. Britt, E. Oveisi, W. L. Queen, *ACS Cent. Sci.* **2018**, *4*, 349.
- [18] J. P. Yang, Q. Li, M. Li, W. B. Zhu, Z. Q. Yang, W. Q. Qu, Y. C. Hu, H. L. Li, *Environ. Sci. Technol.* **2020**, *54*, 2022.
- [19] L. M. Bofi, S. Royuela, F. Zamora, M. L. R. González, J. L. Segura, R. M. Olivas, M. J. Mancheño, *J. Mater. Chem. A* **2017**, *5*, 17973.
- [20] J. T. Wang, Y. W. Hong, Z. C. Lin, C. L. Zhu, J. Da, G. H. Chen, F. Jiang, *Water Res.* **2019**, *160*, 288.
- [21] E. A. Danso, S. Peräniemi, T. Leiviskä, T. Y. Kim, K. M. Tripathi, A. Bhatnagar, *J. Hazard. Mater.* **2020**, *381*, 120871.
- [22] X. Li, Y. Qi, G. Z. Yue, Y. Li, M. C. Zhang, X. H. Guo, X. F. Li, L. J. Ma, S. J. Li, *Green Chem.* **2019**, *21*, 649.
- [23] S. S. Chen, Y. H. Deng, X. Xiao, S. Xu, P. N. Rudd, J. S. Huang, *Nat. Sustain.* **2021**, *4*, 636.
- [24] I. F. Nata, D. R. Wicakso, A. Mirwan, C. Irawan, D. Ramadhani, Ursulla, *J. Environ. Chem. Eng.* **2020**, *8*, 104339.
- [25] Q. Y. Lian, Z. U. Ahmad, D. D. Gang, M. E. Zappi, D. L. Fortela, R. Hernandez, *Chemosphere* **2020**, *248*, 126078.
- [26] Z. L. Li, J. Chen, H. Y. Guo, X. Fan, Z. Wen, M. S. Yeh, C. W. Yu, X. Cao, Z. L. Wang, *Adv. Mater.* **2016**, *28*, 2983.
- [27] A. A. Chavan, H. B. Li, A. Scarpellina, S. Marras, L. Manna, A. Athanassious, D. Fragouli, *ACS Appl. Mater. Interfaces* **2015**, *7*, 14778.
- [28] S. Y. Ding, M. Dong, Y. W. Wang, Y. T. Chen, H. Z. Wang, C. Y. Su, W. Wang, *J. Am. Chem. Soc.* **2016**, *138*, 3031.
- [29] N. Huang, L. P. Zhai, H. Xu, D. L. Jiang, *J. Am. Chem. Soc.* **2017**, *139*, 2428.
- [30] Q. Sun, B. Aguila, J. Perman, L. D. Earl, C. W. Abney, Y. C. Cheng, H. Wei, N. Nguyen, L. Wojtas, S. Q. Ma, *J. Am. Chem. Soc.* **2017**, *139*, 2786.
- [31] D. Zhang, L. Wang, H. H. Zeng, B. Rhimi, C. Y. Wang, *Environ. Sci.: Nano* **2020**, *7*, 793.
- [32] B. L. Chen, L. B. Wang, Y. Q. Xiao, F. R. Fronczek, M. Xue, Y. J. Cui, G. D. Qian, *Angew. Chem., Int. Ed.* **2009**, *48*, 500.
- [33] Y. Z. Jiang, C. Y. Liu, A. S. Huang, *ACS Appl. Mater. Interfaces* **2019**, *11*, 32186.
- [34] Y. Hong, D. Thirion, S. Subramanian, M. Yoo, H. Choi, H. Y. Kim, J. F. Stoddart, C. Yavuz, *Proc. Natl. Acad. Sci. USA* **2020**, *117*, 16174.
- [35] B. Aguila, Q. Sun, J. A. Perman, L. D. Earl, C. W. Abney, R. Elzein, R. Schlaf, S. Q. Ma, *Adv. Mater.* **2017**, *29*, 1700665.
- [36] T. Wu, C. Liu, B. Kong, J. Sun, Y. J. Gong, K. Liu, J. Xie, A. Pei, Y. Cui, *ACS Cent. Sci.* **2019**, *5*, 719.
- [37] G. W. Yang, H. Y. Han, C. Y. Du, Z. H. Luo, Y. J. Wang, *Polymer* **2010**, *51*, 6193.
- [38] J. M. Chalker, M. Mann, M. J. H. Worthington, L. J. Esdaile, *Org. Mater.* **2021**, *3*, 362.
- [39] J. S. M. Lee, D. J. Parker, A. I. Cooper, T. Hasell, *J. Mater. Chem. A* **2017**, *5*, 18603.
- [40] J. L. Wang, Y. S. He, J. Yang, *Adv. Mater.* **2015**, *27*, 569.
- [41] H. H. Yuan, C. Guo, J. H. Chen, H. C. Lu, J. Yang, Y. N. Nuli, J. L. Wang, *J. Energy Chem.* **2021**, *60*, 360.
- [42] K. Y. Wang, S. L. Ju, Q. L. Gao, G. L. Xia, G. F. Wang, H. X. Yan, L. X. Dong, Z. X. Yang, X. B. Yu, *J. Alloys Compd.* **2021**, *860*, 158445.
- [43] Y. L. Ren, J. L. Hu, H. X. Zhong, L. Z. Zhang, *J. Alloys Compd.* **2020**, *837*, 155498.
- [44] A. Benítez, D. D. Lecce, G. A. Elia, Á. Caballero, J. Morales, J. Hassoun, *Adv. Mater.* **2018**, *11*, 1512.
- [45] G. X. Li, J. H. Sun, W. P. Hou, S. D. Jiang, Y. Huang, J. X. Geng, *Nat. Commun.* **2016**, *7*, 10601.
- [46] W. J. Chuang, J. J. Griebel, E. T. Kim, H. Yoon, A. G. Simmonds, H. J. Ji, P. T. Dirlam, R. S. Glass, J. J. Wie, N. A. Nguyen, B. W. Guralnick, J. J. Park, Á. Somogyi, P. Theato, M. E. Mackay, Y. E. Sung, K. Char, J. Pyun, *Nat. Chem.* **2013**, *5*, 518.
- [47] S. Y. Wei, L. Ma, K. E. Hendrickson, Z. Y. Tu, L. A. Archer, *J. Am. Chem. Soc.* **2015**, *137*, 12143.
- [48] S. S. Zhang, *Energies* **2014**, *7*, 4588.
- [49] M. M. Abdallah, M. N. Ahmad, G. Walker, J. J. Leahy, W. Kwapinski, *Ind. Eng. Chem. Res.* **2019**, *58*, 7296.
- [50] K. F. Du, S. K. Li, L. S. Zhao, L. Z. Qiao, H. Ai, X. H. Liu, *ACS Sustainable Chem. Eng.* **2018**, *6*, 17068.
- [51] C. Jin, X. Y. Zhang, J. N. Xin, G. F. Liu, J. Chen, G. M. Wu, T. Liu, J. W. Zhang, Z. W. Kong, *Ind. Eng. Chem. Res.* **2018**, *57*, 7872.
- [52] L. Ding, X. B. Luo, P. H. Shao, J. K. Yang, D. Q. Sun, *ACS Sustainable Chem. Eng.* **2018**, *6*, 8494.
- [53] B. Zhang, J. Li, D. N. Wang, M. L. Feng, X. Y. Huang, *Inorg. Chem.* **2019**, *58*, 4103.
- [54] Y. Li, C. Wang, S. J. Ma, H. Y. Zhang, J. J. Ou, Y. M. Wei, M. L. Ye, *ACS Appl. Mater. Interfaces* **2019**, *11*, 11706.
- [55] Z. Yang, H. W. Liu, J. Li, K. Yang, Z. Z. Zhang, F. J. Chen, B. D. Wang, *ACS Appl. Mater. Interfaces* **2020**, *12*, 15002.
- [56] Z. Qu, L. L. Yan, J. F. Xu, M. M. Liu, Z. C. Li, N. Q. Yan, *ACS Appl. Mater. Interfaces* **2014**, *6*, 18026.
- [57] X. G. Yu, J. Y. Xie, J. Yang, H. J. Huang, K. Wang, Z. S. Wen, *J. Electroanal. Chem.* **2004**, *573*, 121.
- [58] M. Tipplook, P. Pornaroontham, A. Watthanaphanit, N. Saito, *ACS Appl. Nano Mater.* **2020**, *3*, 218.
- [59] J. X. Wang, X. B. Feng, C. W. N. Aderson, X. Ying, L. H. Shang, *J. Hazard. Mater.* **2012**, *221*, 1.
- [60] Y. Fu, Y. Sun, Y. T. Zheng, J. W. Jiang, C. Y. Yang, J. W. Wang, J. S. Hu, *Sep. Purif. Technol.* **2021**, *259*, 118112.
- [61] L. Zhang, J. H. Zhang, X. L. Li, C. J. Wang, A. J. Yu, S. S. Zhang, G. F. Ouyang, Y. Y. Cui, *Appl. Surf. Sci.* **2021**, *538*, 148054.

- [62] W. Qin, G. Y. Qian, H. B. Tao, J. W. Wang, *React. Funct. Polym.* **2019**, *136*, 75.
- [63] F. H. Shen, J. Liu, D. W. Wu, C. K. Gu, Y. C. Dong, *Ind. Eng. Chem. Res.* **2018**, *57*, 7889.
- [64] X. Y. Chen, D. Y. Chen, N. J. Li, Q. F. Xu, H. Li, J. H. He, J. M. Lu, *ACS Appl. Mater. Interfaces* **2020**, *12*, 39227.
- [65] J. H. Ma, G. Y. Zhou, L. Chu, Y. T. Liu, C. B. Liu, S. L. Luo, Y. F. Wei, *ACS Sustainable Chem. Eng.* **2017**, *5*, 843.
- [66] X. Y. He, T. Zhang, Q. Yue, Y. L. Zhou, H. L. Wang, N. S. Bolan, R. Jiang, D. C. W. Tsang, *Sci. Total Environ.* **2021**, *778*, 146116.
- [67] S. Pavithra, G. Thandapani, S. Sugashini, P. N. Sudha, H. H. Alkhamis, A. F. Alrefaei, M. H. Almutairi, *Chemosphere* **2021**, *271*, 129415.
- [68] H. Cao, P. Yang, T. Ye, M. Yuan, J. S. Yu, X. X. Wu, F. Q. Yin, Y. Li, F. Xu, *Chemosphere* **2021**, *278*, 130369.
- [69] M. Luo, Y. Liu, J. C. Hu, H. Liu, J. L. Li, *ACS Appl. Mater. Interfaces* **2012**, *4*, 1813.

# ADVANCED FUNCTIONAL MATERIALS

## Supporting Information

for *Adv. Funct. Mater.*, DOI: 10.1002/adfm.202105845

Reusable Polyacrylonitrile-Sulfur Extractor of Heavy  
Metal Ions from Wastewater

*Peng Li, Haibin Jiang, Ariel Barr, Zhichu Ren, Rui Gao,  
Hua Wang, Weiwei Fan, Meifang Zhu, Guiyin Xu,\* and  
Ju Li\**

## **Supplementary Information for**

### **Reusable polyacrylonitrile-sulfur extractor of heavy metal ions from wastewater**

Peng Li, Haibin Jiang, Ariel Barr, Zhichu Ren, Rui Gao, Hua Wang, Weiwei Fan, Meifang Zhu,  
Guiyin Xu\*, Ju Li\*

Guiyin Xu and Ju Li

Email: [xuguiyin@mit.edu](mailto:xuguiyin@mit.edu); [liju@mit.edu](mailto:liju@mit.edu)

This PDF file includes:

SI Table S1- S3, Fig. S1-S14, and  
SI references

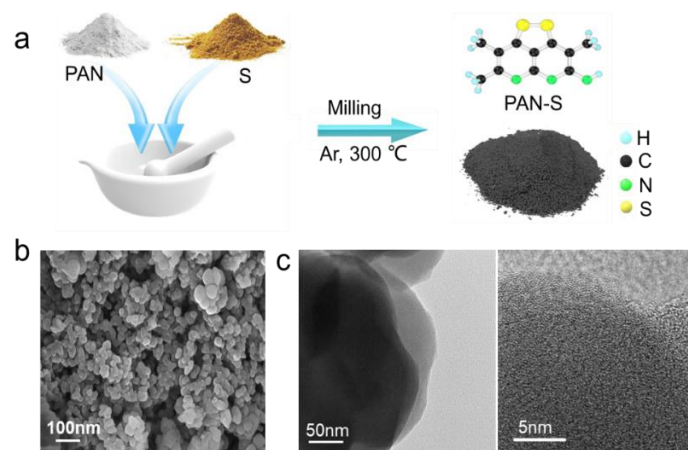


**Fig. S1** Preparation illustration (a), SEM (b) and TEM (c) images of the PAN-S nanoparticle.

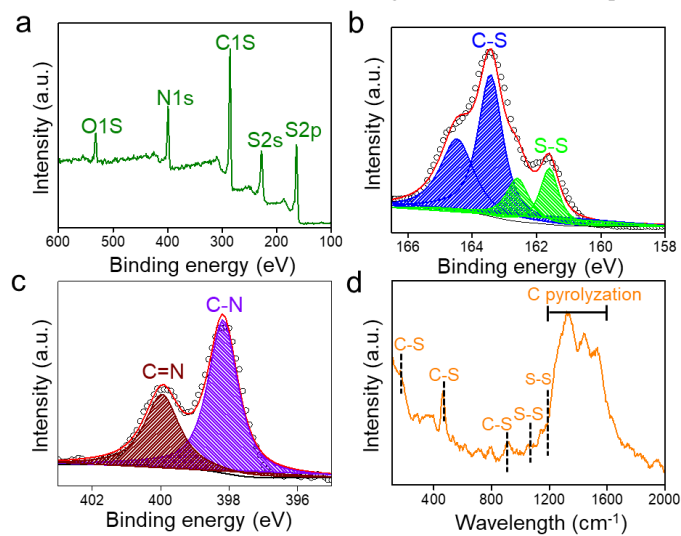


**Fig. S2** The XPS spectrum (a), S 2p (b) and N 1s (c) high resolution scanning XPS spectrum, and Raman spectrum (d) of PAN-S nanoparticles.

Calculation of  $K_d$  values for adsorption of different metal ions by PAN-S nanoparticles

**Table S1** Experiment results for mixed metal ion adsorption ( $K_d$  value calculation)

	Hg <sup>2+</sup>	Pb <sup>2+</sup>	Cu <sup>2+</sup>	Cd <sup>2+</sup>	Zn <sup>2+</sup>	Ca <sup>2+</sup>	Ni <sup>2+</sup>	Mn <sup>2+</sup>	Mg <sup>2+</sup>	Fe <sup>3+</sup>	Al <sup>3+</sup>
Initial <sup>a</sup>	103.82	69.84	40.69	78.76	82.36	97.44	76.29	68.46	108.74	16.86	69.71
Terminal <sup>b</sup>	0.006	0.57	0.87	21.74	75.17	93.35	74.63	67.76	101.85	14.77	59.55
R%	99.99	99.18	97.86	72.40	8.73	4.20	2.18	1.02	0.63	12.39	14.57
Error%	3.22	2.46	4.61	2.96	2.43	1.26	0.11	0.20	0.13	2.22	3.42
$K_d$	1666	1653	1631	1206	145	69	36	17	105	206	242

a, b: Initial and Terminal indicating the initial and terminal concentration of the metal ions,  $\mu\text{g/L}$ ;

R%, removal efficiency;

Error%, represents systematic errors in measurements;

$K_d$  is the distribution coefficient, mL/g.

Experimental condition: To prepare the Hg<sup>2+</sup>, Cu<sup>2+</sup>, Pb<sup>2+</sup>, Cd<sup>2+</sup>, Zn<sup>2+</sup>, Ca<sup>2+</sup>, Ni<sup>2+</sup>, Mn<sup>2+</sup>, Mg<sup>2+</sup>, Fe<sup>3+</sup>, and Al<sup>3+</sup> mixture solution, 100.0  $\mu\text{g/L}$  concentration of species was used and the solution pH was adjusted to 5.0. The initial mixture is set aside for 24 hours, then passed through a 0.22  $\mu\text{m}$  filter membrane. The result of this process is then treated as the initial “waste-water” solution in the adsorption experiments. The adsorption experiment is conducted at a temperature of 25 °C for a 2.0 h duration using 50.0 mL of the waste-water solution to which a 30.0 mg dosage of PAN-S has been added.

PAN-S show superior affinity for Hg<sup>2+</sup>, Pb<sup>2+</sup>, Cu<sup>2+</sup>, and Cd<sup>2+</sup> ions. The  $K_d$  values for Hg<sup>2+</sup>, Pb<sup>2+</sup>, Cu<sup>2+</sup>, Cd<sup>2+</sup> ions were 1666, 1653, 1631, and 1206 mL/g, respectively, which are much larger than that for Zn<sup>2+</sup>, Ca<sup>2+</sup>, Ni<sup>2+</sup>, Mn<sup>2+</sup>, Mg<sup>2+</sup>, Fe<sup>3+</sup>, and Al<sup>3+</sup> species. This result indicates a superior selectivity of PAN-S towards Hg<sup>2+</sup>, Pb<sup>2+</sup>, Cu<sup>2+</sup>, and Cd<sup>2+</sup> ions.

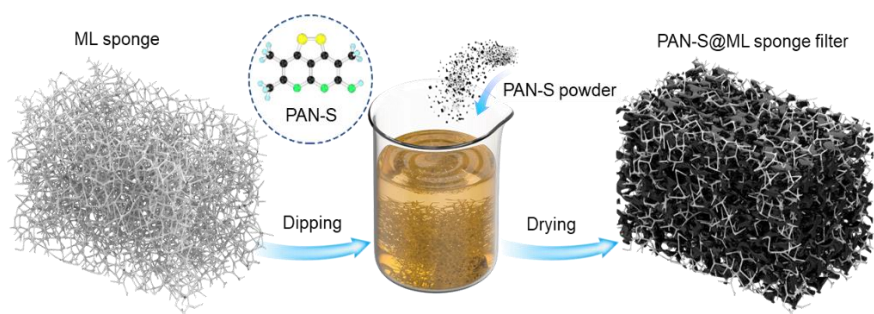


**Fig. S3** Illustration of PAN-S@ML sponge filter fabrication with a facial dipping and drying process.

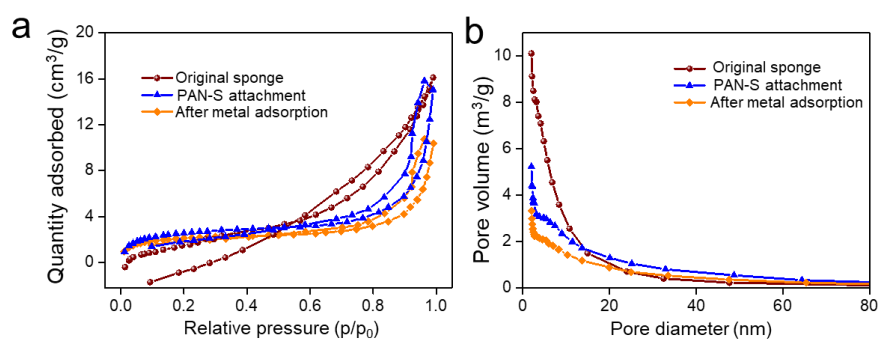


**Fig. S4** Nitrogen adsorption-desorption isotherms (a) and the pore size distribution (b) of the original sponge, PAN-S@ML sponge, and PAN-S@ML sponge after Hg<sup>2+</sup> adsorption.

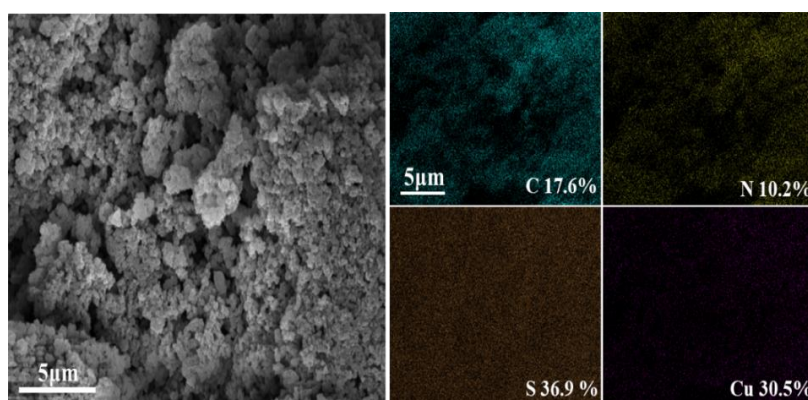


**Fig. S5** SEM-mapping results of PAN-S@ML sponge after Cu<sup>2+</sup> flow-through adsorption. Experimental condition: Cu<sup>2+</sup> initial concentration of 60.0 mg/L, the wastewater volume of 300 mL, adsorption pH of 7.0, 5.0, 5.0, and 7.0, repeated 3 times.

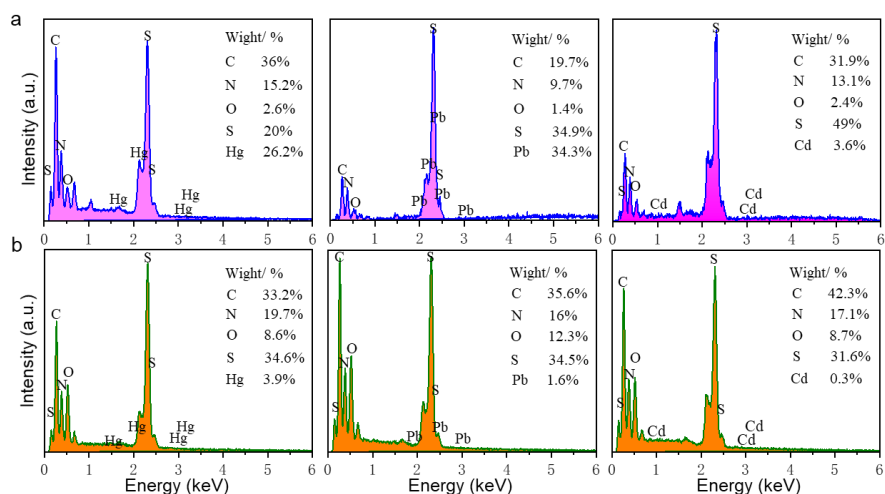


**Fig. S6** EDS results of Hg<sup>2+</sup>, Pb<sup>2+</sup>, and Cd<sup>2+</sup> on PAN-S@ML sponge surface (a) and the corresponding EDS results after Hg<sup>2+</sup>, Pb<sup>2+</sup>, and Cd<sup>2+</sup> electro-desorption treatment (b).

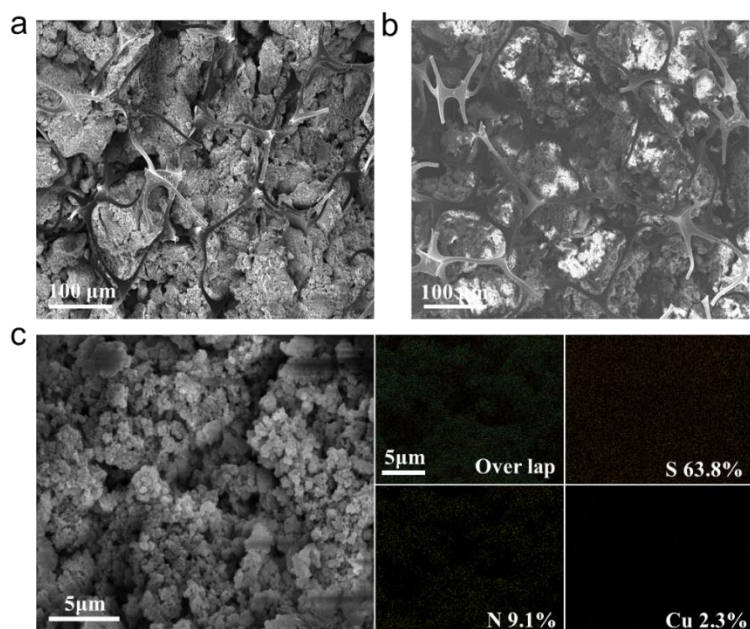


**Fig. S7** SEM images of PAN-S@ML sponge after Cu<sup>2+</sup> adsorption (a) and electro-desorption (b). SEM-mapping images and corresponding element distribution of PAN-S@ML sponge after Cu<sup>2+</sup> electro-desorption (c).



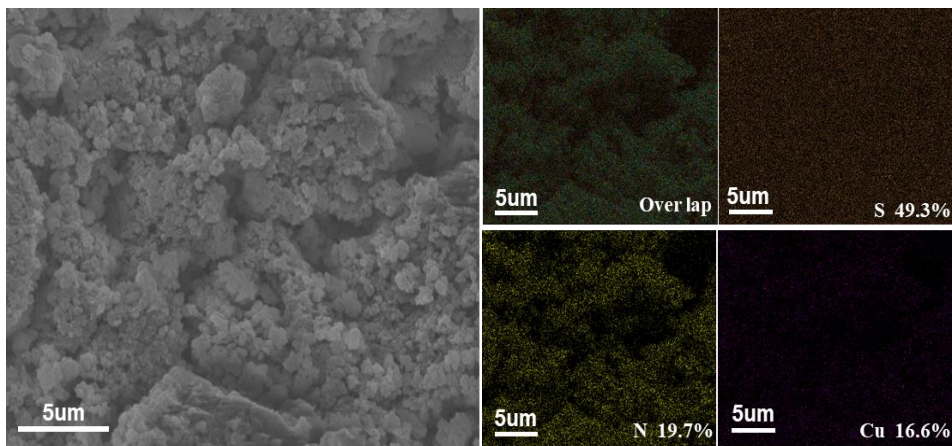


**Figure S8** SEM-mapping images and corresponding element distribution of PAN-S@ML sponge after  $\text{Cu}^{2+}$  elution with 0.5 mol/L  $\text{HNO}_3$  solution

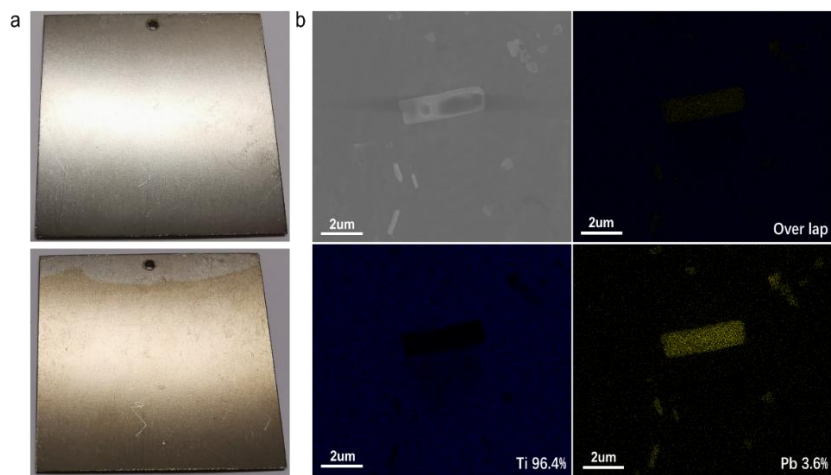


**Fig. S9** Digital photos of Ti cathode before (up in **a**) and after  $\text{Cu}^{2+}$  adsorbed PAN-S@ML sponge electro-desorption (down in **a**) and SEM images of Ti cathode after  $\text{Pb}^{2+}$  adsorbed PAN-S@ML sponge electro-desorption and the corresponding SEM-mapping results (**b**).

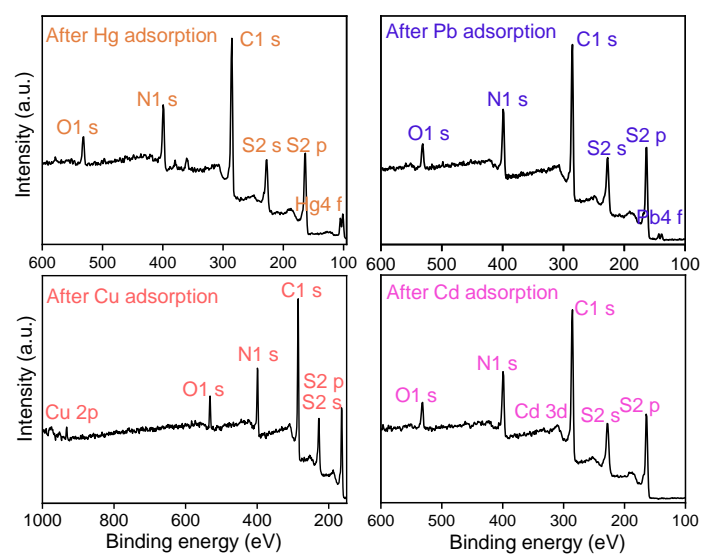


**Fig. S10** XPS spectra of PAN-S after  $\text{Hg}^{2+}$ ,  $\text{Pb}^{2+}$ ,  $\text{Cu}^{2+}$ , and  $\text{Cd}^{2+}$  adsorption. Experimental condition: metal ion concentration of 10.0 mg/L, pH=5.0, PAN-S dosage of 30.0 mg, wastewater volume of 50 mL, adsorption duration of 24 h, and temperature of 25 °C

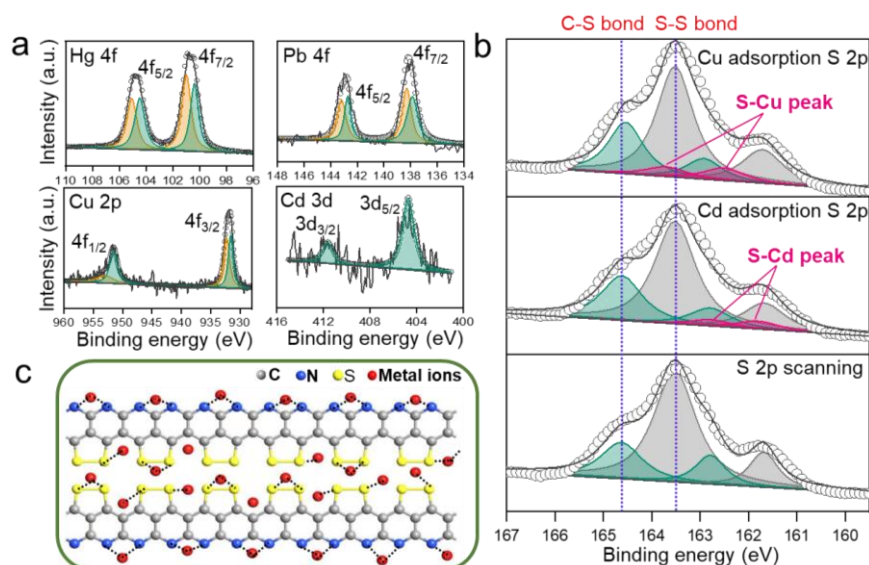


**Fig. S11** High resolution XPS spectra for Hg 4f, Pb 4f, Cu 2p and Cd 3d (a), the high resolution XPS spectra of S 2p after Cu<sup>2+</sup> and Cd<sup>2+</sup> adsorption (b), and the illustration of proposed metal ion adsorption mechanism of PAN-S (c). Experimental condition: metal ion concentration of 10.0 mg/L, pH=5.0, PAN-S dosage of 30.0 mg, wastewater volume of 50 mL, adsorption duration of 24 h, and temperature 25 °C.

The high resolution XPS spectrum for Pb 4f demonstrated the existence of N-Pb and S-Pb interaction from the Pb 4f<sub>7/2</sub> binding energy peaks at 138.28 and 137.86 eV, and Pb 4f<sub>5/2</sub> binding energy peaks located at 143.19 and 142.72 eV, respectively.<sup>[1,2]</sup> After Cu<sup>2+</sup> adsorption, the high resolution XPS for Cu 2p also indicated the existence of N-Cu and S-Cu bonds. From the binding energy peaks of Cu 2p<sub>3/2</sub> and Cu 2p<sub>1/2</sub> at 931.55 and 951.54 eV, N-Cu interaction can be inferred. Moreover, the binding energy peaks of Cu 2p<sub>3/2</sub> and Cu 2p<sub>1/2</sub> at 932.25 and 953.05 eV demonstrate the adsorption of Cu<sup>2+</sup> by an -S bond on the PAN-S surface.<sup>[3,4]</sup> The Cd 3d high resolution XPS spectrum was disordered and blurry. This may be ascribed to the relatively weak interaction between Cd<sup>2+</sup> and PAN-S, and the low initial Cd<sup>2+</sup> concentration in the wastewater. The S-Cd bond can still be found through the binding energy peaks at 404.31 and 411.66 eV (**Fig. S11a**).<sup>[5]</sup>

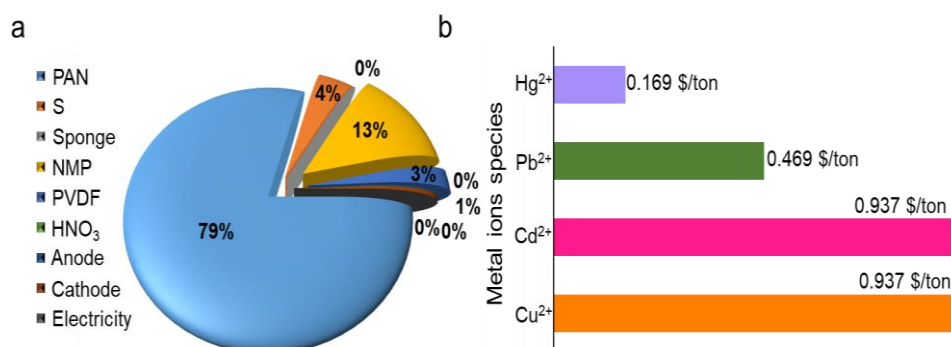
**Table S2** Cumulative economic demand of the PAN-S@ML sponge engineered with 8.0 g PAN-S.

Item	Price/ (US \$/unit)	From	Amount	Cost (\$)	Ref.
PAN	4.0 \$/G	Sigma	6.0 G	24.0	6
S	0.055 \$/G	Sigma	24.0 G	1.32	7
Sponge	0.01 \$/G	Amazon	0.2 G	0.002	8
NMP	0.05 \$/G	Sigma	80 G	4.0	9
PVDF	1.0 \$/G	Sigma	0.8 G	0.8	10
0.5 M HNO <sub>3</sub>	0.00002 \$/mL	Sigma	150 mL	0.003	11
Graphite	10 \$/m <sup>2</sup>	Yinyi. Co China	6*6 cm <sup>2</sup>	0.036	12
Ti Cathode	50 \$/m <sup>2</sup>	Qixin Co. China	6*6 cm <sup>2</sup>	0.18	13
Electricity fees	6.55/kwh	USA	0.000175 kwh	0.001	14
Total				30.369	

**Table S3** Hg<sup>2+</sup>, Pb<sup>2+</sup>, Cu<sup>2+</sup>, and Cd<sup>2+</sup> metal ions polluted wastewater treatment cost.

Item	<sup>a</sup> Concentration	<sup>b</sup> EPA	Cost (US \$/ton)
Hg <sup>2+</sup> water	5 ppb	2 ppb	0.169
Pb <sup>2+</sup> water	5 ppb	0 ppb	0.469
Cd <sup>2+</sup> water	10 ppb	5 ppb	0.937
Cu <sup>2+</sup> water	1500 ppb	1300 ppb	0.937

- a. Initial concentration of the Hg<sup>2+</sup>, Pb<sup>2+</sup>, Cd<sup>2+</sup>, and Cu<sup>2+</sup> contaminated surface/ground water, which may be regarded as a potential drinking water source, was assumed to be 5, 5, 10, and 1500 ppb.
- b. EPA means the US Environmental Protection Agency regulation for Hg<sup>2+</sup>, Pb<sup>2+</sup>, Cd<sup>2+</sup>, and Cu<sup>2+</sup>.

**Fig. S12** Economic cost percentage of different components (a) and the treatment cost for Hg<sup>2+</sup>, Pb<sup>2+</sup>, Cd<sup>2+</sup>, and Cu<sup>2+</sup> contaminated wastewater (b). In consideration of the ultra-robust stability of the PAN-S@ML, we assumed the reuse times as 20.

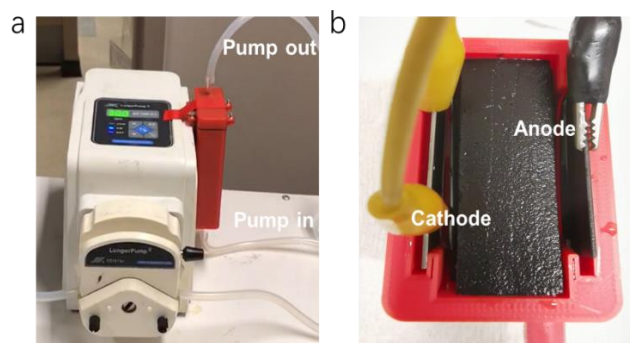


**Fig. S13** Photos of self-designed flow-through adsorption (a) and electro-desorption (b) devices. Dimensions of the flow-through device: 60 mm length, 20 mm width, 120 mm height. Dimensions of the electro-desorption device: 60 mm length, 30 mm width, 60 mm height, and the electrode distance of 25 mm.

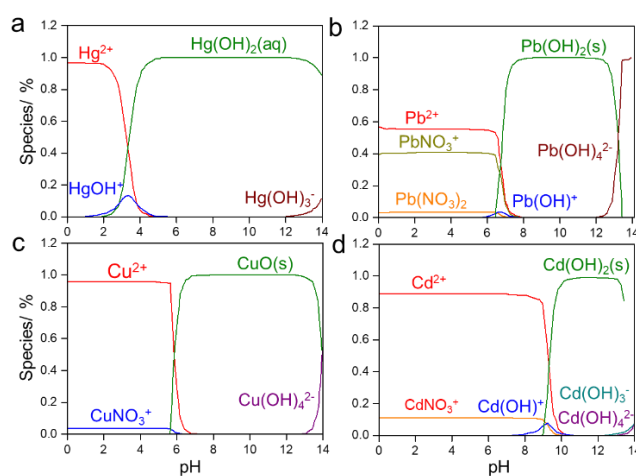


**Fig. S14**  $\text{Hg}^{2+}$  (a),  $\text{Pb}^{2+}$  (b),  $\text{Cu}^{2+}$  (c), and  $\text{Cd}^{2+}$  (d) species distribution with nitrate anion as a function of pH simulated with  $\text{Hg}^{2+}$ ,  $\text{Pb}^{2+}$ ,  $\text{Cu}^{2+}$ , and  $\text{Cd}^{2+}$  concentration of 5.0, 3.0, 60.0, and 3.0 mg/L,  $\text{NO}_3^-$  concentration of 0.05 mol/L (Calculated by Visual MINTEQ 3.1).

## Reference

1. X. Y. Chen, D. Y. Chen, N. J. Li, Q. F. Xu, H. Li, J. H. He, J. M. Lu, *ACS Appl. Mater. Interfaces* 2020, **12**, 39227.
2. J. H. Ma, G. Y. Zhou, L. Chu, Y. T. Liu, C. B. Liu, S. L. Luo, Y. F. Wei, *ACS Sustainable Chem. Eng.* 2017, **5**, 843–851.
3. X. Y. He, T. Zhang, Q. Xue, Y. L. Zhou, H. L. Wang, N. S. Bolan, R. F. Jiang, D. C. W. Tsang, *Sci. Total Environ.* 2021, **778**, 146116.
4. S. Pavithra, G. Thandapani, S. Sugashini, P. N. Sudha, H. H. Alkhamis, A. F. Alrefaei, M. H. Almutairi, *Chemosphere* 2021, **271**, 129415.
5. M. Luo, y. Liu, J. C. L. Hu, H. Liu, J. J. Li, *ACS Appl. Mater. Interfaces* 2012, **4**, 1813.
6. Sigmaaldrich. Website for polyacrylonitrile prices. <https://www.sigmaaldrich.cn/CN/zh/search/%E8%81%9A%E4%B8%99%E7%83%AF%E8%85%88?focus=products&page=1&perPage=30&sort=relevance&term=%E8%81%9A%E4%B8%99%E7%83%AF%E8%85%88&type=product> (2021).
7. Sigmaaldrich. Website for sulfur powder prices. <https://www.sigmaaldrich.cn/CN/en/search/sulfur?focus=products&page=1&perPage=30&sort=relevance&term=sulfur&type=product> (2021).
8. Amazon. Website for melamine sponge prices. [https://www.amazon.com/-/zh/dp/B08CK98BTG/ref=sr\\_1\\_6?\\_\\_mk\\_zh\\_CN=%E4%BA%9A%E9%A9%AC%E9%80%8A%E7%BD%91%E7%AB%99&dchild=1&keywords=melamine+Sponge&qid=1620288561&sr=8-6](https://www.amazon.com/-/zh/dp/B08CK98BTG/ref=sr_1_6?__mk_zh_CN=%E4%BA%9A%E9%A9%AC%E9%80%8A%E7%BD%91%E7%AB%99&dchild=1&keywords=melamine+Sponge&qid=1620288561&sr=8-6) (2021).
9. Sigmaaldrich. Website for N-methyl-pyrrolidinone prices. <https://www.sigmaaldrich.cn/CN/en/search/n-methyl-pyrrolidinone?focus=products&page=1&perPage=30&sort=relevance&term=N-methyl-pyrrolidinone&type=product> (2021).
10. Sigmaaldrich. Website for polyvinylidene fluoride prices. <https://www.sigmaaldrich.cn/CN/en/search/polyvinylidene-fluoride?focus=products&page=1&perPage=30&sort=relevance&term=polyvinylidene%20fluoride&type=product> (2021).
11. Sigmaaldrich. Website for nitric acid prices. <https://www.sigmaaldrich.cn/CN/en/search/nitric-acid?focus=products&page=1&perPage=30&sort=relevance&term=Nitric%20acid&type=product> (2021).
12. Li, P. et al. Highly efficient interception and precipitation of uranium (VI) from aqueous solution by iron-electrocoagulation combined with cooperative chelation by organic ligands. *Environ. Sci. Technol.* 2017, **51**, 14368–14378.
13. P. Li, et al. Ternary semiconductor metal oxide blends grafted Ag@AgCl hybrid as dimensionally stable anode active layer for photoelectrochemical oxidation of organic compounds: Design strategies and photoelectric synergistic mechanism. *J. Hazard. Mater.* 2019, **362**, 336–347.
14. Electric power monthly. Table 5.6.A. US average price of electricity to ultimate customers by end-use sector. [https://www.eia.gov/electricity/monthly/epm\\_table\\_grapher.php?t=epmt\\_5\\_6\\_a](https://www.eia.gov/electricity/monthly/epm_table_grapher.php?t=epmt_5_6_a) (2020).